Chapter 1

Induction Generator in Wind Power Systems

Yu Zou

Additional information is available at the end of the chapter

http://dx.doi.org/10.5772/60958

Abstract

Wind power is the fastest growing renewable energy and is promising as the number one source of clean energy in the near future. Among various generators used to convert wind energy, the induction generator has attracted more attention due to its lower cost, lower requirement of maintenance, variable speed, higher energy capture efficiency, and improved power quality [1-2]. Generally, there are two types of induction generators widely used in wind power systems – Squirrel-Cage Induction Generator (SCIG) and Doubly-Fed Induction Generator (DFIG). The straightforward power conversion technique using SCIG is widely accepted in fixed-speed applications with less emphasis on the high efficiency and control of power flow. However, such direct connection with grid would allow the speed to vary in a very narrow range and thus limit the wind turbine utilization and power output. Another major problem with SCIG wind system is the source of reactive power; that is, an external reactive power compensator is required to hold distribution line voltage and prevent whole system from overload. On the other hand, the DFIG with variable-speed ability has higher energy capture efficiency and improved power quality, and thus dominates the large-scale power conversion applications. With the advent of power electronics techniques, a back-to-back converter, which consists of two bidirectional converters and a dc-link, acts as an optimal operation tracking interface between DFIG and loads [3-5]. Field orientation control (FOC) is applied to both rotor- and stator-side converters to achieve desirable control on voltage and power [6,7].

In this chapter, a brief introduction of wind power system is presented first, which is followed by introduction of SCIG and DFIG from aspects of modeling and control. The basic FOC algorithm is derived based on DFIG model in *dq* reference frame. At last, the power generation efficiency is considered through different Maximum Power Point Tracking (MPPT) methods that have attracted a lot of attention in the variable-

speed operation systems. A comparative analysis involving advantage and disadvantage of the methods is conducted.

Keywords: wind power systems, SCIG, DFIG, back-to-back converter, FOC, MPPT

1. Introduction

The core component of a modern induction generator wind power system is the turbine nacelle, which generally accommodates the mechanisms, generator, power electronics, and control cabinet. The mechanisms, including yaw systems, shaft, and gear box, etc., facilitate necessary mechanical support to various dynamic behavior of the turbine. The generator is dedicated to the conversion between mechanical energy, which is captured by turbine rotor, and electrical energy. The generated electrical energy then needs to be regulated and conditioned to be connected to the power grid for use. In this section, the wind power system layout and classification are introduced first, which is followed by the outlining of the feasible power electronic converter interface between generators and loads. Lastly, the control scheme is briefly addressed and discussed in detail in section 2.

1.1. Overview of wind power systems

Figure 1 shows the general layout of a wind turbine nacelle. The generator is either driven (in generation mode) or propelling (in motoring mode) the turbine blades through a shaft. The gearbox can be used to facilitate the speed difference between turbine and generator. The blade stall and pitch mechanisms are also involved to limit the power as well as the turbine plane yawing and tilting. By these means, the blade effective aerofoil cross section and thus the interface with wind pressure can be controlled. The performance coefficients responding to different yaw angle and pitch angle show significant variations [1-3]. In addition, as the most dynamically efficient choice, three blades connected through a hub with flanges is the commonly used topology in the front of the nacelle. The flanges are designed to enable the pitch angle adjustment. In most of the variable-speed wind systems, the high-efficiency operation always relies on the wind speed information. As a result, the anemometer can be used as one of the solutions. The basic function of the tower is to reach a higher position in order to obtain more airstream and wind speed. The tower can be constructed in either soft or stiff ways. A stiff tower has a natural frequency which lies above the blade passing frequency. Soft towers are lighter and cheaper but have to withstand more movement, and thus suffer from higher stress levels [2].

There are a number of classifications that group the wind power systems into different categories. According to the loads, grid integrated system and islanded system are employed to feed power grid and isolated load, respectively. According to the generators used, popular options are SCIG wind system, DFIG wind system, and Permanent Magnet Synchronous Generator (PMSG) wind system. Other alternative generator systems are also mentioned in

http://dx.doi.org/10.5772/60958

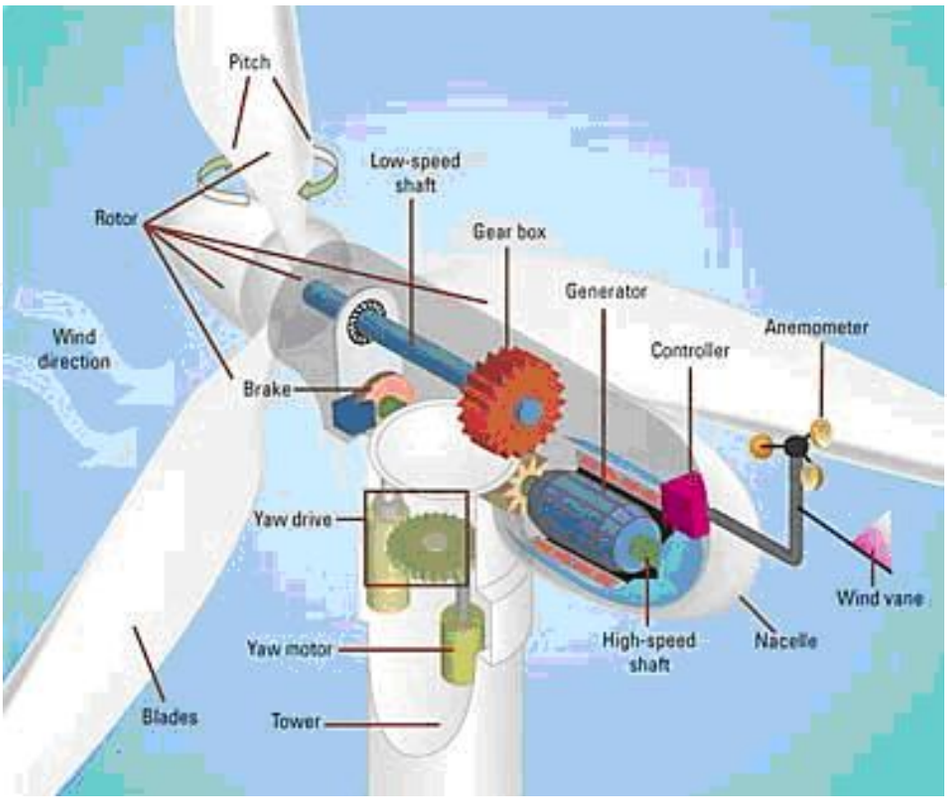

Figure 1. Wind power system nacelle [8]

the literature, such as brushless DFIGs (BDFIG) system [5,6], direct-drive synchronous generator (DDSG) system [7,9], switched reluctance generator (SRG) system [10], multiple-stage geared SCIG system [10], and radial/axial/transversal-flux PM generator systems [7,12-14]. These solutions generally require relatively complex operation principle and equipment assembly. According to the presence of the gear box, there are multistage gear box wind system, single-stage gear box wind system, and direct drive wind system (without gear box) in where the Synchronous Generator (SG) qualifies the system to have a simpler and more reliable drive train. However, the lower generator speed, and thus larger torque, requires more poles, larger diameter, and volume, and hence higher cost.

The most promising classifications in induction generator wind systems are fixed-speed, limited-variable-speed, and variable-speed wind systems, according to the operations of induction generator speed. Comparisons between these wind power systems have been intensively conducted, based on different speed variation levels [12,15-19]. A summary of their advantages and disadvantages is presented in Table 1. The fixed-speed concept has been successfully applied in SCIG wind systems. The drive train applies multiple-stage gearbox and a SCIG is directly connected to the grid via a transformer. To support the grid, external reactive power compensation and soft starter are necessary [5,6]. The limited variable-speed system is an improved version of the SCIG type but it uses a wound rotor induction generator instead, which allows the stator to be connected to the grid, and the rotor to have a variable resistance controlled by a power converter. Through the control of rotor resistance, the slip of the

generator is varied. The variable-speed system is a concept commonly used in large power rating applications (>1.5 MW). Different combinations among DFIG, SCIG, partial or full converters would lead to variable-speed operation systems. The control system maintains the optimal generator speed, thus the optimal output power, through controlling the generator currents and voltages. Due to the high efficiency and capability of Faults Ride Through (FRT), this type of wind power system dominates the high-capacity power market nowadays.

	Advantages	**Disadvantages**
Fixed-speed system	a. Simple construction and robust b. Low cost and maintenance c. Easy control	a. Not optimal operation, thus low efficiency b. Easy power fluctuation caused by wind speed and tower pressure c. External reactive power compensation is needed d. Weak capability of FRT
Limited-speed system	a. Limited speed variation is implemented b. The slip ring may be replaced by optical coupling	a. Speed variation range depends on the size of the variable rotor resistance (<10%) b. The controlled rotor power must be dissipated by heat in the resistor c. Still need reactive power compensation and cannot support the grid alone
Variable-speed system	a. Large range of speed variation b. Appropriate control enables optimal operation for maximum power extraction c. No external power compensation is needed and is able to support the grid d. High FRT capability e. Suitable and commonly used for large-scale wind farms	a. Relatively complicated control system b. Higher converters and control costs c. May need a multistage gearbox and slip ring in DFIG system d. May need expensive PM material and large diameter design in direct drive

Table 1. Comparison among different wind power systems

1.2. Power electronics interface topologies in wind power systems

Power electronics is the key element enabling the regulation and conditioning of the power, voltage, and frequency with high efficiency and flexibility. In addition, more involvement of distributed power systems nowadays emphasizes the crucial role of power electronics interface among energy generation, storage, and transmission.

Due to the developments in semiconductor switches and microprocessors, many power electronics techniques have been developed during the past decades [20,21]. Besides the diode converters, line-commutated thyristor converters and self-commutated IGBT/MOSFET converters are found applicable to wind power systems. The line-commutated converters are generally used in high-power applications but they are incapable of controlling the reactive

power. The self-commutated converters are able to transfer and control power bidirectionally because of the capability of controllable switch turning-off. Nowadays, wind power systems, especially the variable-speed wind power system, primarily rely on the converters that implement full power control. Different converter topologies and combinations have been successfully employed in this field, as shown in Figure 2.

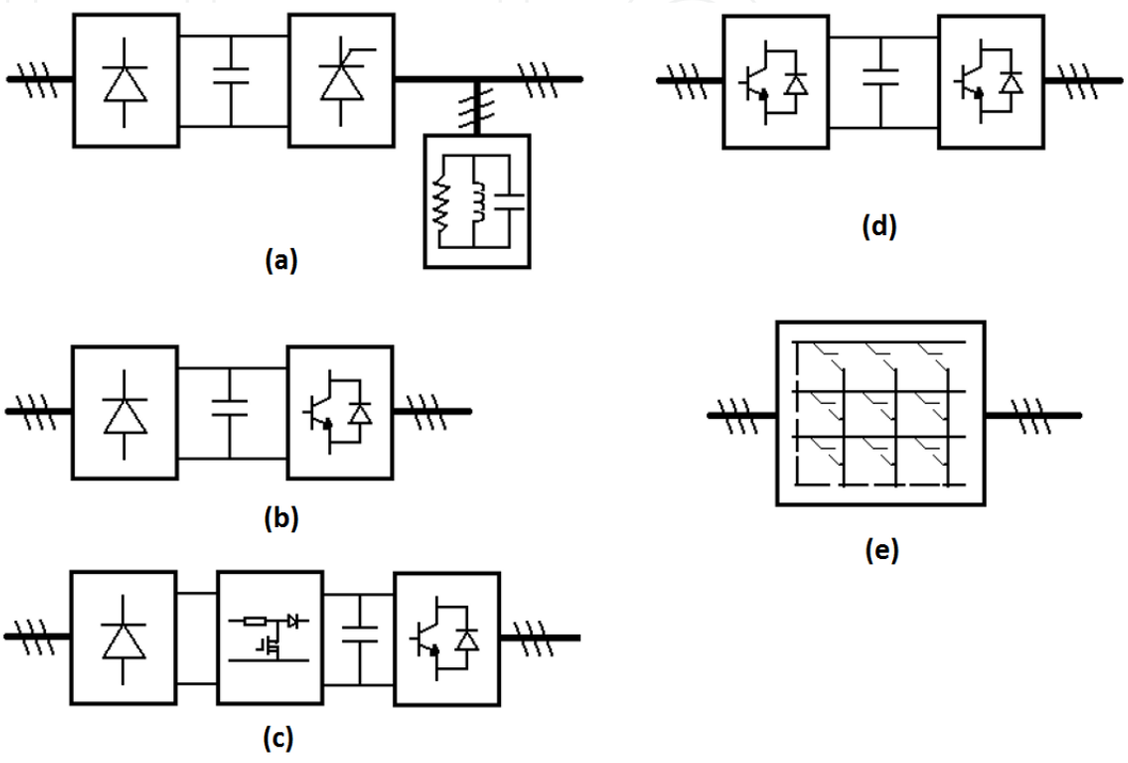

Figure 2. Commonly used power electronics converter topologies for wind power system ((a) diode and line-commutated converter, combined with reactive power compensation; (b) diode and PWM VSI converter; (c) diode and DC/DC chopper and PWM VSI converter; (d) back-to-back PWM VSI converter; (e) matrix converter)

Due to the employment of diode rectifier, the topology in Figure 2(a) is uncontrolled and a thyristor inverter is used to regulate the generator speed through dc-link voltage to obtain firing angle commands. Obviously, this scheme is simple for control and costs less than self-commutated converter. More importantly, it is suitable for high power rating applications. However, the weakness is that extra reactive power compensation is required, which contains a voltage source converter (VSC). The grid voltage may be regulated to obtain reference current for the compensator and the control signal comes from the regulation of the compensator current [22,23]. To remove the compensator, a self-commutated converter could be used to take the place of thyristor inverter, as shown in Figure 2(b). Again, the regulation of dc-link voltage can provide current reference, which is controlled to generate control signals for the PWM inverter [24]. Two self-commutated converters connected through a dc-link, as shown in Figure 2(d), enable bidirectional power flow, which is the key to ensuring high efficiency in motoring operation of generator. The FOC is applied on both sides of converters based on *dq* reference frame [23,25]. The grid-side converter keeps a constant dc-link voltage, while the

generator-side converter is responsible for both active and reactive power control [23]. In the generator-side converter control, the *d*-axis current could be set at zero to maximize the torque, while the *q*-axis current is derived from power regulation [26,27]. An alternative topology of Figure 2(d) is shown in Figure 2(c), where the generator-side self-commutated converter is replaced by a diode rectifier connected to an intermediate chopper [28]. This configuration is impossible for bidirectional power flow caused by the diode rectifier. But it can achieve a similar wide range of speed variation as two self-commutated converters. The grid-side converter controls the dc-link voltage for *d*-axis current reference and controls the reactive power for *q*-axis current reference. The active power regulation and thus the speed control are carried out to generate reference dc-link current. The duty cycle of chopper switch can be obtained using current regulation. The converter configurations discussed are actually multistage implementation of AC conversion. An intermediate DC stage is needed to assist conversion and associated control. In recent years, such procedure has been investigated by a single-stage converter, the matrix converter, which performs the energy transformation without help from a bulky storage stage. The controllable switches are arranged in such a way that any input phase may be connected to any output phase at any time. The matrix converter may be applied to the DFIG system, like the topology in Figure 2(e) [29,30]. According to the stator flux FOC, the reactive and active power can be regulated by *d*- and *q*-axis current, respectively [30]. An alternative control strategy is by regulating the rotor winding voltage to control the power factor (PF) and applying the double space vector PWM technique [29]. It is worth noting that the SCIG system has high starting currents. One effective way to limit the starting current is by using the soft-starter that applies thyristors to limit the RMS starter current below rated current. The starter is shorted after the full load is reached. The torque peak can be decreased as well, which reduces the gearbox pressure [9,10].

The high-efficiency energy conversion and full control of power exclusively rely on the power electronic converter and the control scheme applied on. Consequently, the broadly accepted total wind power system topologies subject to above power electronics are reviewed as follows. Since the high-efficiency variable speed systems are the primary focus, Figure 3 summarizes the feasible variable-speed system topologies, for induction generator systems as well as synchronous generator systems for systematized purpose. Due to the low demand on the converter power rating of approximately 30% of the total power rating, the DFIG with partial converter, shown in Figure 3(a), is a widespread topology for wind power systems. Also, due to the presence of a rotor-side converter, the rotor power is fed back to the grid without dissipation in the resistor. Instead of a partial converter, PMSG or SCIG can be connected to a full rating converter, as shown Figure 3(b). This topology has better grid FRT ability because the generator-side is totally independent of the grid-side. However, the converter rating and loss are high. Figure 3(c) shows the direct drive system, which is aimed at removing the gearbox and associated loss [16]. The generator rotor is connected to the turbine shaft directly and runs at the same very slow speed. Therefore, a high torque and a large machine radius are required to transfer the same amount of power. Fewer components enable less loss and thus more reliable performance in this type of system. To compromise between machine size and spinning speed, the single-stage gearbox, shown in Figure 3(d), is applied [15]. Figure 3(e) shows the electrically excited synchronous generator (EESG) system, which has a rotor-side

http://dx.doi.org/10.5772/60958

converter to provide DC excitation while the stator is connected to a full converter like the case in Figure 3(c). Although there is an increase in cost due to the extra winding for excitation and it also requires more maintenance, the EESG could minimize the loss through controlling the flux via rotor converter [7,11,12].

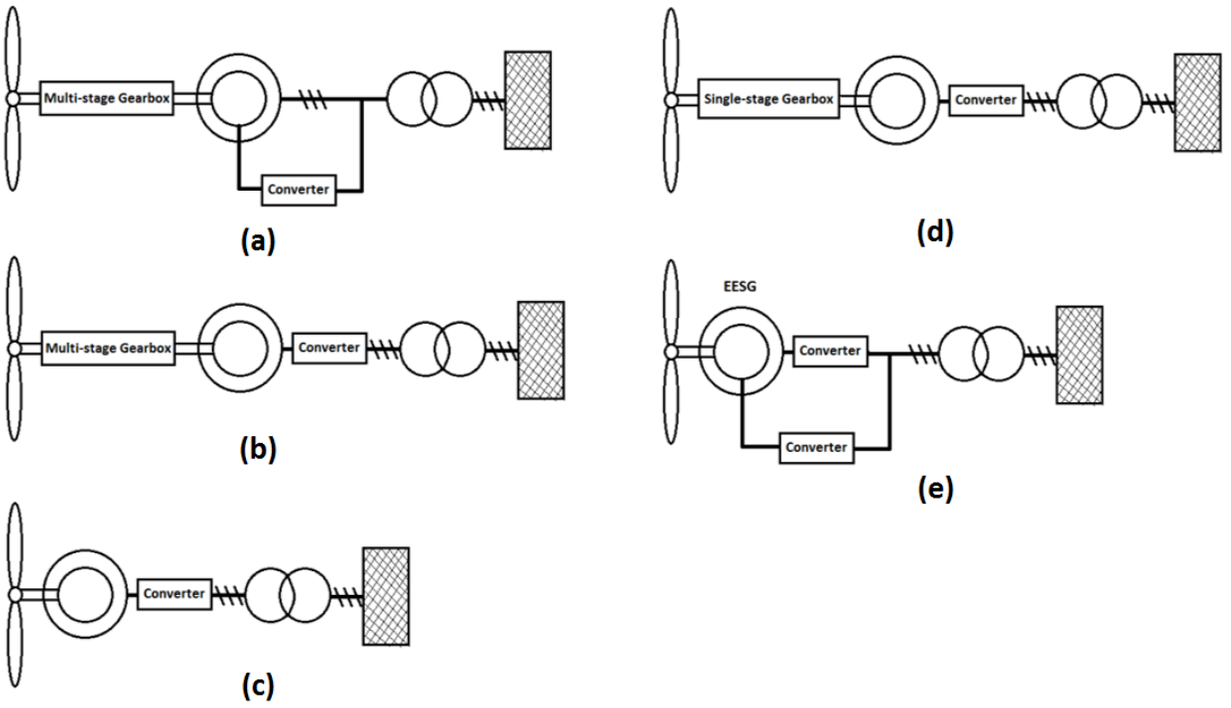

Figure 3. Commonly used wind power system topologies ((a) DFIG with partial/matrix converter; (b) PMSG/SCIG with full converter; (c) direct drive; (d) PMSG with full converter and less stage gearbox; (e) EESG direct drive)

1.3. Generator control schemes in wind power systems

SCIG and DFIG are used almost exclusively in the energy conversion stage of the induction generator wind power system. The most commonly used system topologies are SCIG directly connected into the power grid and DFIG fed by back-to-back converter (Figure 3(a) and Figure 3(d)). The first topology implies a constant frequency and voltage of the SCIG that establishes a fixed-speed operation. In such system, the SCIG relies on the grid (or capacitor bank) to provide reactive power which is necessary to build electromagnetic excitation for rotary field. The generating mode of SCIG is triggered by driven torque which acts opposite to the generator speed within the super-synchronous speed operation region. Due to the absence of the power electronics interface, such system can only serve the grid support applications, wherein just limited control (pitch angle control) can be applied.

The DFIG system, on the other hand, enables the flexible and efficient operations with FOC applied on the rotor-winding-side power electronics interface. The FOC is an instantaneous control that effectively manipulates the position-dependent variables, such as torque and power, in induction generator wind power systems. By aligning a particular space variable

with *d*-axis, stator currents could be decoupled into flux component and torque component in *dq* rotating frame. The currents can be thus controlled separately like in DC motor drive. To implement the control in hardware, PWM technique is generally employed based on Space Vector Modulation (SVM). The SVM is based on space reference voltage vector and associated switching logics. Any space vector can be comprised of vector sum of two adjacent voltage vectors, and the duty cycles of three-phase voltages are calculated based on the dwelling time of two voltage vectors. This is the method widely used in standard industry applications.

The following section examines the detailed modeling and control strategies of both systems.

2. Model and control of induction generator in wind power systems

2.1. Model of wind power and wind turbine

As a typical kinetic energy, wind energy is extracted through wind turbine blades and then transferred by the gearbox and rotor hub to mechanical energy in shaft. The shaft drives the generator to convert the mechanical energy to electrical energy. According to Newton's law, the kinetic energy for the wind with particular wind speed V_w is described as:

$$E_k = \frac{1}{2} m V_w^{\ 2} \tag{1}$$

where m represents the mass of the wind, and its power can be written as:

$$P_w = \frac{\partial E_k}{\partial t} = \frac{1}{2}\frac{\partial m}{\partial t} V_w^{\ 2} = \frac{1}{2}\left(\rho A V_w\right) V_w^{\ 2} = \frac{1}{2}\rho A V_w^{\ 3} \tag{2}$$

where ρ and A are the air density and turbine rotor swipe area, respectively. The extracted mechanical power can thus be expressed as:

$$P_m = C_p\left(\lambda,\ \beta\right) P_w = C_p\left(\lambda,\ \beta\right)\frac{1}{2}\rho A V_w^{\ 3} \tag{3}$$

where P_m is the mechanical output power in watt, which depends on performance coefficient $C_p(\lambda, \beta)$, C_p depends on tip speed ratio λ and blade pitch angle β, and determines how much of the wind kinetic energy can be captured by the wind turbine system. A nonlinear model describes $C_p(\lambda, \beta)$ as [3]:

$$C_p\left(\lambda,\ \beta\right) = c_1\left(c_2 - c_3\beta - c_4\beta^2 - c_5\right)e^{-c_6} \tag{4}$$

http://dx.doi.org/10.5772/60958

where, c_1=0.5, c_2=116/λ_i, c_3=0.4, c_4=0, c_5=5, c_6=21/λ_i and

$$\lambda_i = \frac{1}{\lambda + 0.08\beta} - \frac{0.035}{\beta^3 + 1} \tag{5}$$

With the dependence on the λ and β, maximum value of C_p could be reached and maintained through controlling the pitch angle and generator speed at particular wind speed. A group of typical $C_p - \lambda$ curves for different β is shown in Figure 4 and there is always a maximum value for C_p at one particular wind speed. Correspondingly, the output power is determined by different C_p and also the generator speed at different wind speed, as shown in Figure 5, where there is always one maximum power value for each wind speed, which is the goal of the MPPT control.

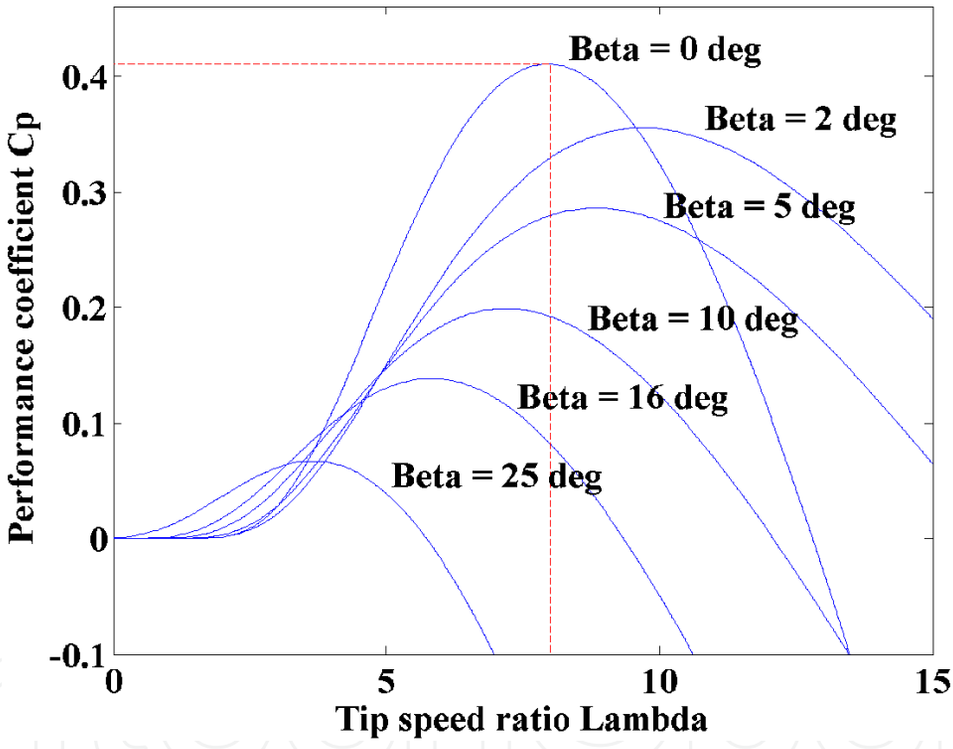

Figure 4. C_p versus λ curve for a wind turbine (β is the pitch angle) [23]

2.2. Model and control of SCIG

As a fixed-speed wind power system, SCIG is directly connected to the grid through transformer and thus operates at almost constant speed without controlling from power electronics interface. It was commonly used in Denmark during 1980s and 1990s and thus is also called "Danish Concept" system. The robust and simple configuration qualifies such system for many applications where the cost is a higher priority concern than efficiency. Figure 6 shows the schematics of entire SCIG wind system including the wind turbine, pitch control, and reactive

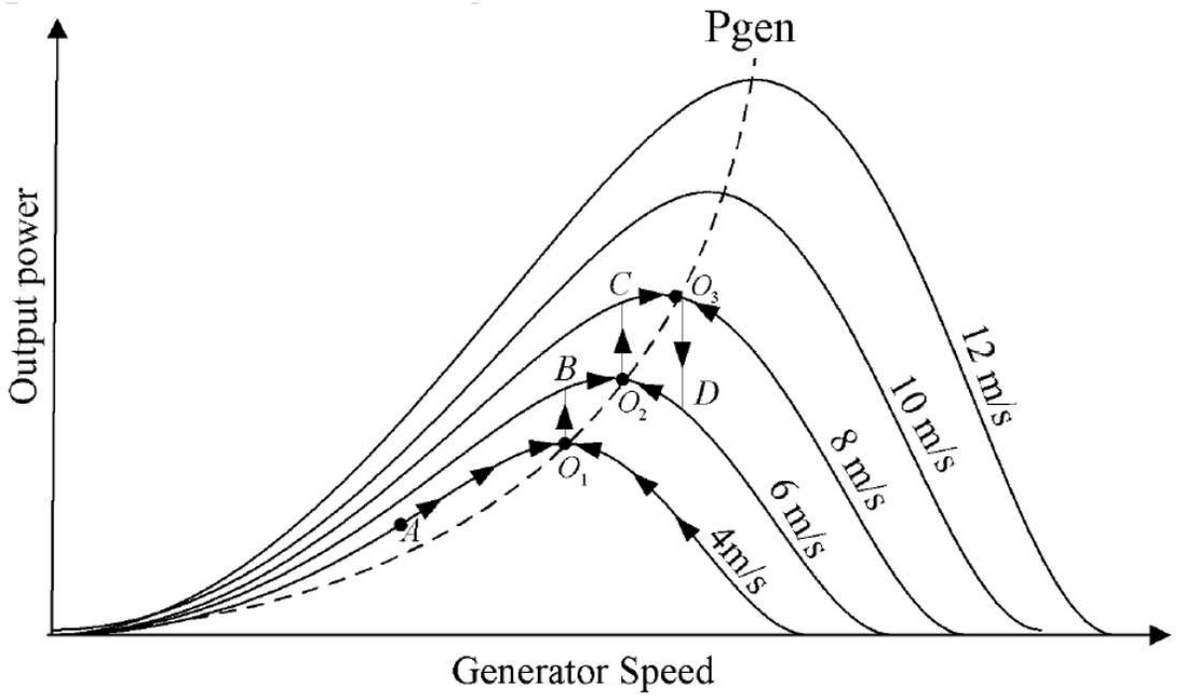

Figure 5. Power versus generator speed curve for wind turbine [31]

power compensator. The entire system includes three stages for delivering the energy from wind turbine to the power grid. The first one is wind farm stage which handles with low-voltage V_{wt}; the second is distribution stage which has medium-voltage V_{dis}; the third is grid transmission stage which has high-voltage V_{grid}. The three-phase transformers take care of the interface between two stages [10]. The nominal power is considered as active power reference to regulate the pitch angle, while the distribution line-to-line voltage and phase current are monitored to favor the reactive power compensation for distribution line. This fairly straightforward technique was firstly used since it is simple, with rugged construction, has reliable operation and is low cost. However, the fixed-speed nature and potential voltage instability problem severely limit the operations of SCIG wind system [1,3].

It is clear from Figure 5 that at a particular wind speed, the output active power is also a fixed value in the case of fixed generator speed. Thus, the output power is exclusively wind speed dependent until the nominal power is reached. The wind speed at nominal power is called nominal wind speed. Beyond this wind speed, the pitch angle system will prevent the output power from exceeding the nominal value. The pitch angle is determined by an open-loop control of regulated output active power and, as shown in Figure 7. Due to the huge size of blade and thus the huge inertia, pitch angle has to change at a slow rate and within a reasonable range. It is also worth noting that without reactive power source, the SCIG system tends to a voltage droop in distribution line which will cause overload problem.

Simulation in [23] illustrates the operation of a 0.855MW SCIG system. From Figure 8, the initial generator speed is set at slip s = -0.01 p.u. with respect to synchronous speed and then response to the wind speed input disturbance. Since the power is lower than the nominal value (0.855

http://dx.doi.org/10.5772/60958

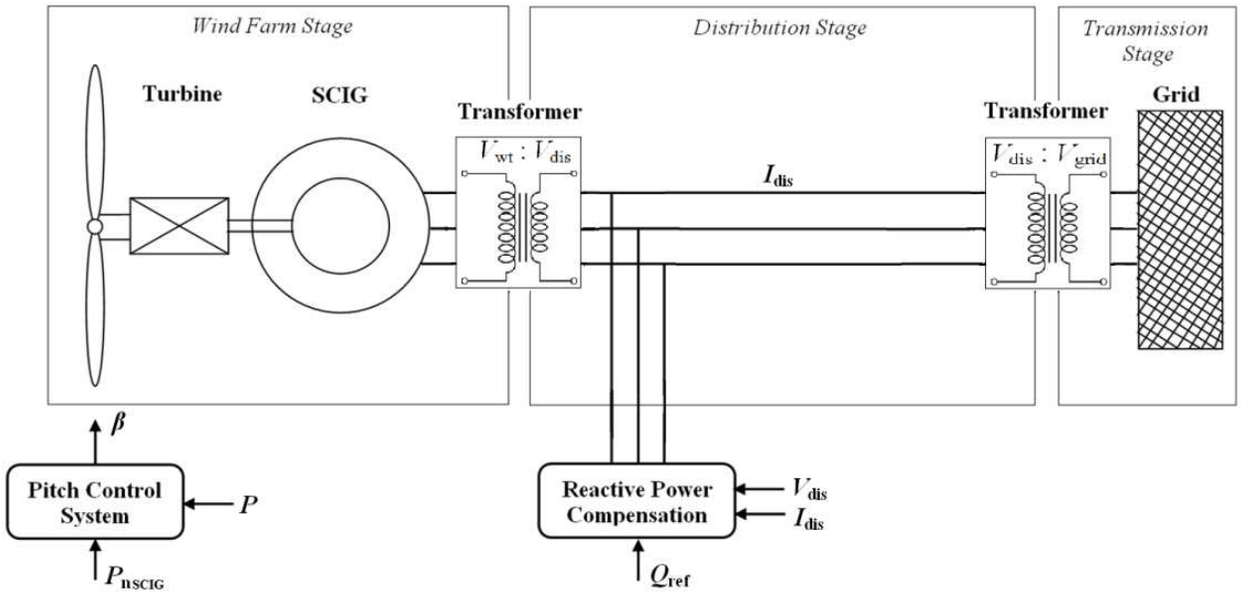

Figure 6. SCIG wind power system configuration

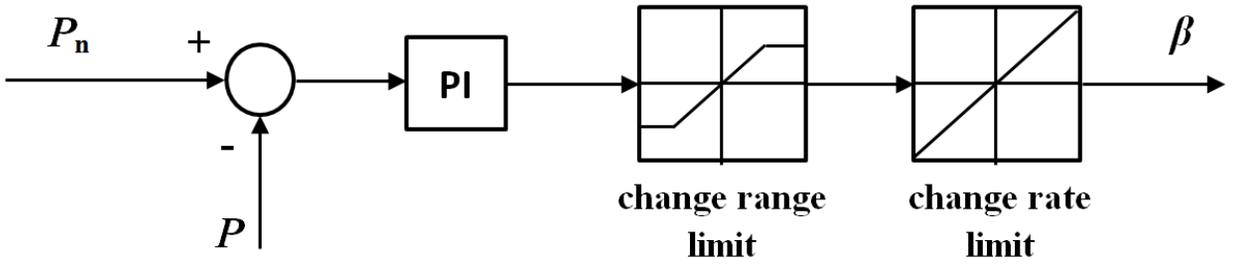

Figure 7. Pitch angle control

MW) before t = 10 s, pitch angle control is not online. Since that moment, the wind speed increases and so do the generator speed and power until the wind speed exceeds the nominal value (11 m/s) at where the pitch control is triggered to block the further increase of output power. In this way, the output power persists at nominal value thereafter.

It is noted that the generator speed can only vary in very small range around 1 p.u. and thus it is impossible to attain the optimal output power. Also, without independent control ability, SCIG system consumes reactive power of 0.41 Mvar at the steady state, which will lead to line voltage droop. To provide necessary reactive power, a Static Synchronous Compensator (STATCOM) is applied in distribution line. As in Figure 9, distribution line voltage can drop by approximately 0.055 p.u. in SCIG system without STATCOM, which will be a potential induction of overload in system. In contrast, SCIG system with STATCOM can hold distribution voltage at 0.99 p.u., which is favorable to grid system stability. The compensated reactive power from STATCOM is shown in Figure 10 and is equal to 0.3 Mvar at the steady state. Although STACOM provides impressive help to a constant distribution line voltage, DFIG wind system presents more attractive attributes.

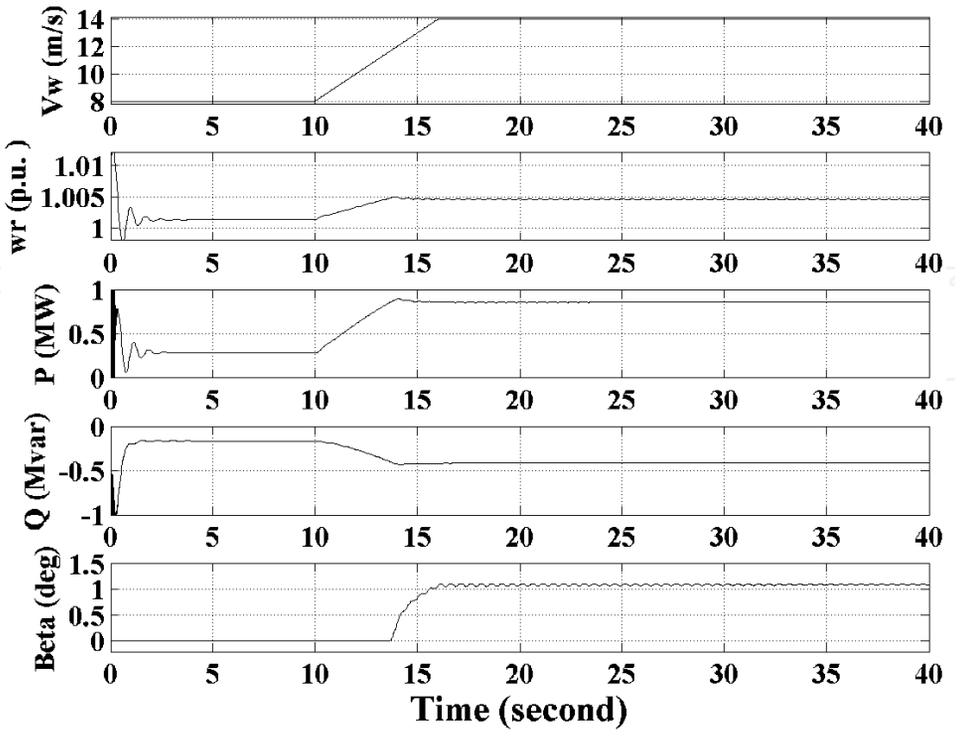

Figure 8. Pitch angle control for SCIG system [23]

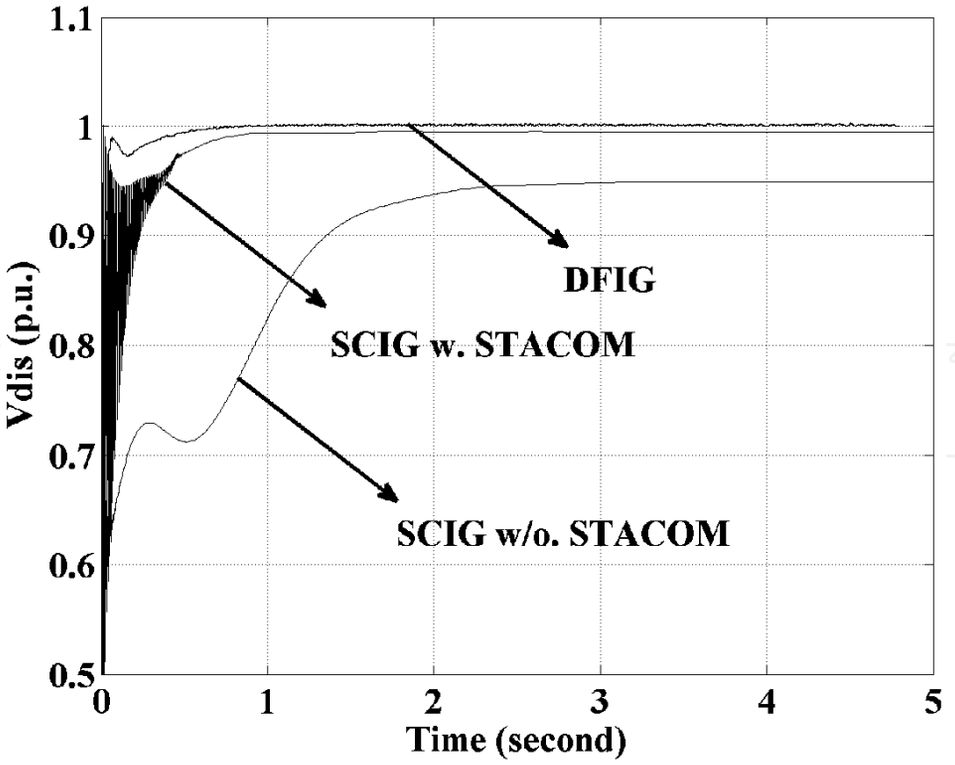

Figure 9. Grid voltages comparison between SCIG w/o. STACOM, SCIG w. STACOM and DFIG [23]

http://dx.doi.org/10.5772/60958

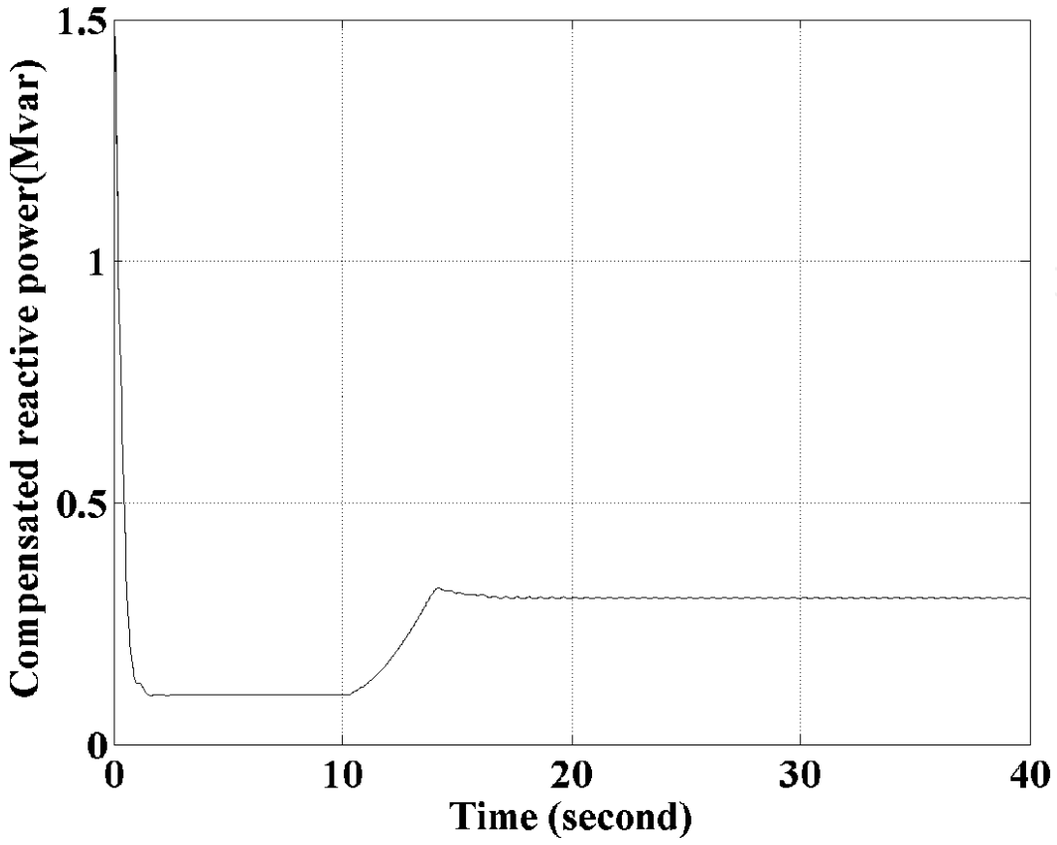

Figure 10. Compensated reactive power from STATCOM [23]

2.3. Model and control of DFIG

Traditionally, the dynamic slip control is employed to fulfill the variable-speed operation in induction generator wind system, in which the rotor windings are connected with variable resistor and control the slip by varied resistance [3,11]. This type of system attains limited variations of generator speed but external reactive power source is still necessary. In order to completely remove the reactive power compensation and control both active and reactive power independently, DFIG wind power system is one of most popular methods in wind energy applications [1,3,7]. The DFIG wind power system with associated back-to-back converter is a typical variable speed system as shown in Figure 11, which complies with the topologies in Figures 3(a) and 2(d). The generator stator windings are connected directly to grid (with fixed voltage and frequency of grid) while the rotor windings are fed by an AC/DC/AC IGBT-based PWM converter (back-to-back converter with capacitor dc-link), at variable frequency through slip rings and brushes. Although such system needs the gearbox and slip rings to function, many advantages enable DFIG system to dominate most wind market nowadays. It facilitates variation of a wide speed range (±30% around synchronous speed), the lower rating requirement on power converters (30% of generator power), and thus lower cost. Also, it has high efficiency induced by bidirectional power flow, and the ability to perform reactive power compensation and smooth grid integration. In this configuration, the back-to-

back converter consists of two parts: the stator/grid-side converter and the rotor-side converter. Both are voltage source converters while a capacitor bank between two converters acts as a dc voltage interface.

In this section, the modeling of DFIG is introduced first and followed by the consequent FOC algorithm which is divided into two parts: stator-side converter control and rotor-side converter control. The SVM method and islanded operation control are also addressed.

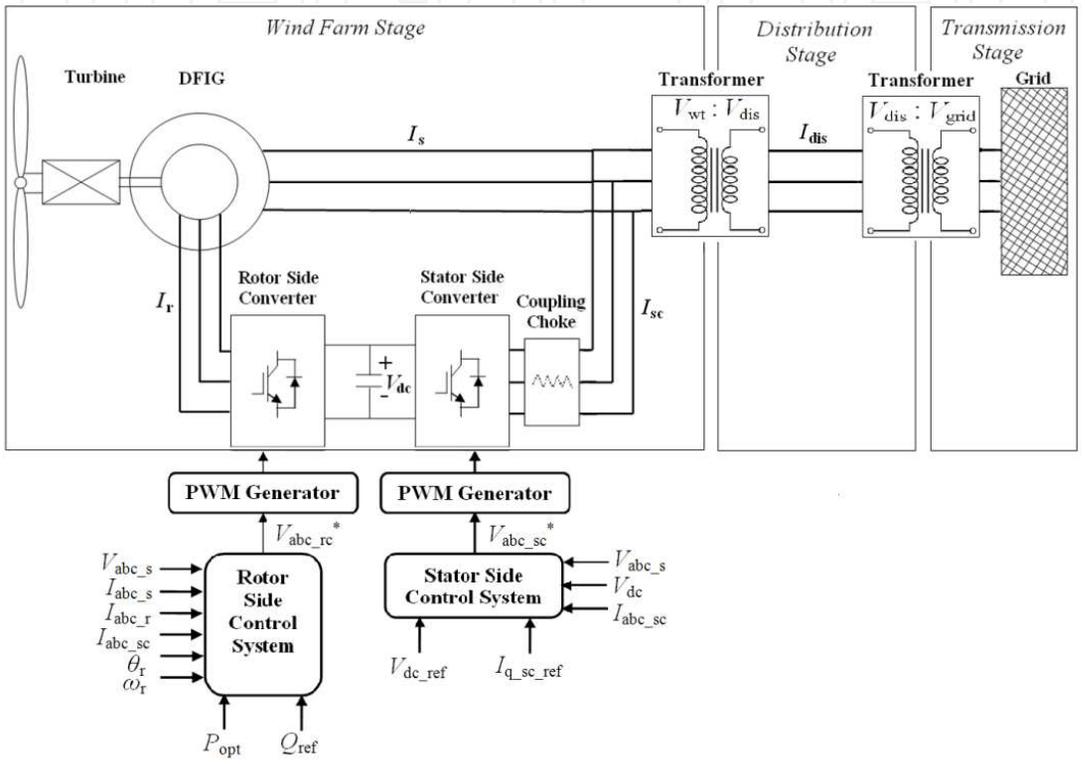

Figure 11. DFIG wind power system configuration

2.3.1. dq model of DFIG

The modeling is conducted under the *dq* reference frame. The equivalent circuits of DFIG in the *dq* reference frame are depicted in Figure 12(a, b) and the relationships between voltage V, current *I*, flux Ψ, and torque T_e can be derived by writing KVL equations. For stator-side, the *d*- and *q*-axis voltage components are given as:

$$\begin{aligned} V_{ds} &= R_s I_{ds} - \omega_s \Psi_{qs} + \left(L_{ls} + L_m\right)\frac{dI_{ds}}{dt} + L_m \frac{dI_{dr}}{dt} a \\ V_{qs} &= R_s I_{qs} + \omega_s \Psi_{ds} + \left(L_{ls} + L_m\right)\frac{dI_{qs}}{dt} + L_m \frac{dI_{qr}}{dt} b \end{aligned} \tag{6}$$

And similarly, the *d*- and *q*-axis voltage components in rotor-side are given as:

http://dx.doi.org/10.5772/60958

$$V_{dr} = R_r I_{dr} - s\omega_s \Psi_{qr} + \left(L_{lr} + L_m\right)\frac{dI_{dr}}{dt} + L_m \frac{dI_{ds}}{dt} a$$
$$V_{qr} = R_r I_{qr} + s\omega_s \Psi_{dr} + \left(L_{lr} + L_m\right)\frac{dI_{qr}}{dt} + L_m \frac{dI_{qs}}{dt} \; b \tag{7}$$

Because the flux linkage along *d*- and *q*-axis follow:

$$\Psi_{ds} = L_s I_{ds} + L_m I_{dr} \; a$$
$$\Psi_{qs} = L_s I_{qs} + L_m I_{qr} \; b \tag{8}$$

$$\Psi_{dr} = L_r I_{dr} + L_m I_{ds} \; a$$
$$\Psi_{qr} = L_r I_{qr} + L_m I_{qs} \; b \tag{9}$$

The reorganized DFIG stator voltages in *d*- and *q*-axis, respectively, are presented as:

$$V_{ds} = R_s I_{ds} - \omega_s \Psi_{qs} + \frac{d\Psi_{ds}}{dt} a$$
$$V_{qs} = R_s I_{qs} + \omega_s \Psi_{ds} + \frac{d\Psi_{qs}}{dt} b \tag{10}$$

And the DFIG rotor voltages in *d*- and *q*-axis, respectively, are presented as:

$$V_{dr} = R_r I_{dr} - s\omega_s \Psi_{qr} + \frac{d\Psi_{dr}}{dt} a$$
$$V_{qr} = R_r I_{qr} + s\omega_s \Psi_{dr} + \frac{d\Psi_{qr}}{dt} b \tag{11}$$

The generator electromagnetic torque is correspondingly given as:

$$T_e = \frac{3}{2} n_p \left(\Psi_{ds} I_{qs} - \Psi_{qs} I_{ds}\right) \tag{12}$$

where $L_s = L_{ls} + L_m$; $L_r = L_{lr} + L_m$; and $s\omega_s = \omega_s - \omega_r$ represents the difference between synchronous speed and generator speed; subscripts r, s, m, d, q denote the rotor, stator, magnitizing, *d*-axis and *q*-axis components, respectively; T_e is electromagnetic torque; L_m and n_p are generator mutual inductance and the number of pole pairs, respectively.

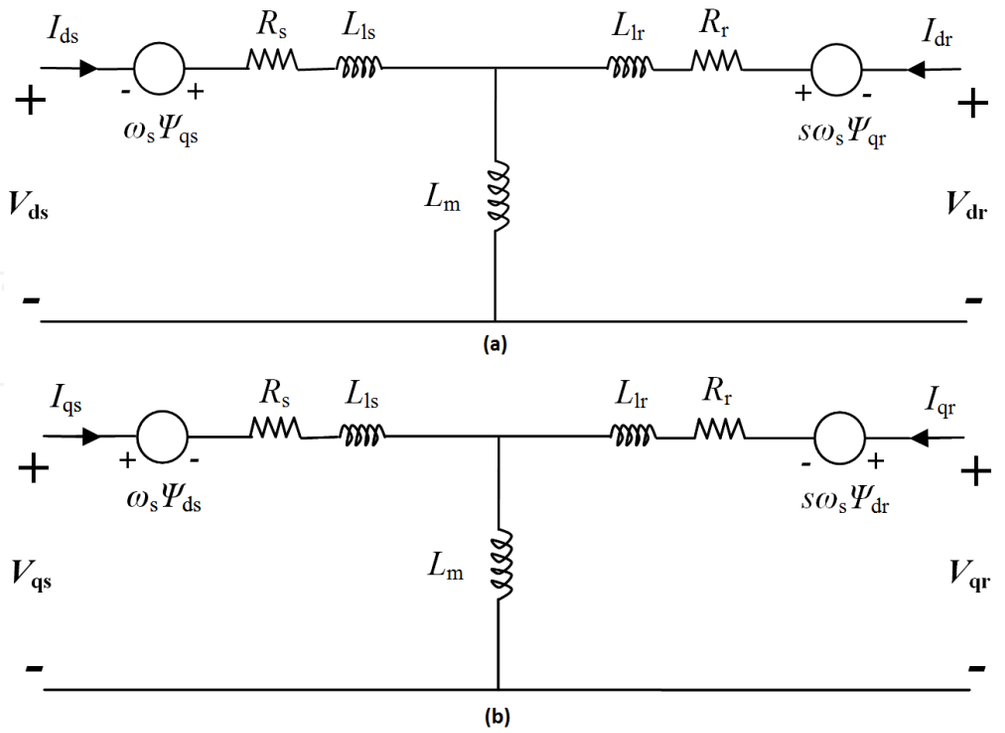

Figure 12. Equivalent circuit of DFIG ((a) *d*-axis; (b) *q*-axis)

2.3.2. Control of rotor-side converter

The control of DFIG modeled above is applied on back-to-back converter and is therefore also divided into rotor-side control and stator-side control.

First, the rotor-side converter is studied. To *d*-axis, the rotor flux linkage Ψ_{qr} in Equation (7a) is substituted by Equation (9b), resulting in:

$$V_{dr} = R_r I_{dr} - s\omega_s \left(L_r I_{qr} + L_m I_{qs}\right) + \frac{d\left(L_r I_{dr} + L_m I_{ds}\right)}{dt} \tag{13}$$

By substituting the I_{ds} by Ψ_{ds} in Equation (8a), the Equation (13) can be expressed as:

$$V_{dr} = R_r I_{dr} - s\omega_s L_r I_{qr} - s\omega_s L_m I_{qs} + L_r \frac{dI_{dr}}{dt} + \frac{L_m}{L_s} \frac{d\left(\Psi_{ds} - L_m I_{dr}\right)}{dt} \tag{14}$$

Because it is directly connected to the grid, the stator voltage shares constant magnitude and frequency of grid voltage. One could make the *d*-axis align with stator voltage vector, and it is true that V_s=V_{ds} and V_{qs}=0, thus Ψ_s=Ψ_{qs} and Ψ_{ds}=0, which are stator voltage-oriented vector control scheme, as depicted in Figure 13. Therefore, Equation (14) can be organized as:

http://dx.doi.org/10.5772/60958

$$V_{dr} = [R_r + \left(L_r - \frac{L_m^2}{L_s} \right) \frac{d}{dt}] I_{dr} - s\omega_s [L_r I_{qr} + L_m I_{qs}] \tag{15}$$

Equation (15) implies that the *d*-axis rotor voltage consists of two voltage components V_{dr}^1 and V_{dr}^2:

$$\begin{aligned} V_{dr}^1 &= [R_r + \left(L_r - \frac{L_m^2}{L_s} \right) \frac{d}{dt}] I_{dr} \; a \\ V_{dr}^2 &= -s\omega_s \left[L_r I_{qr} + L_m I_{qs} \right] \; b \end{aligned} \tag{16}$$

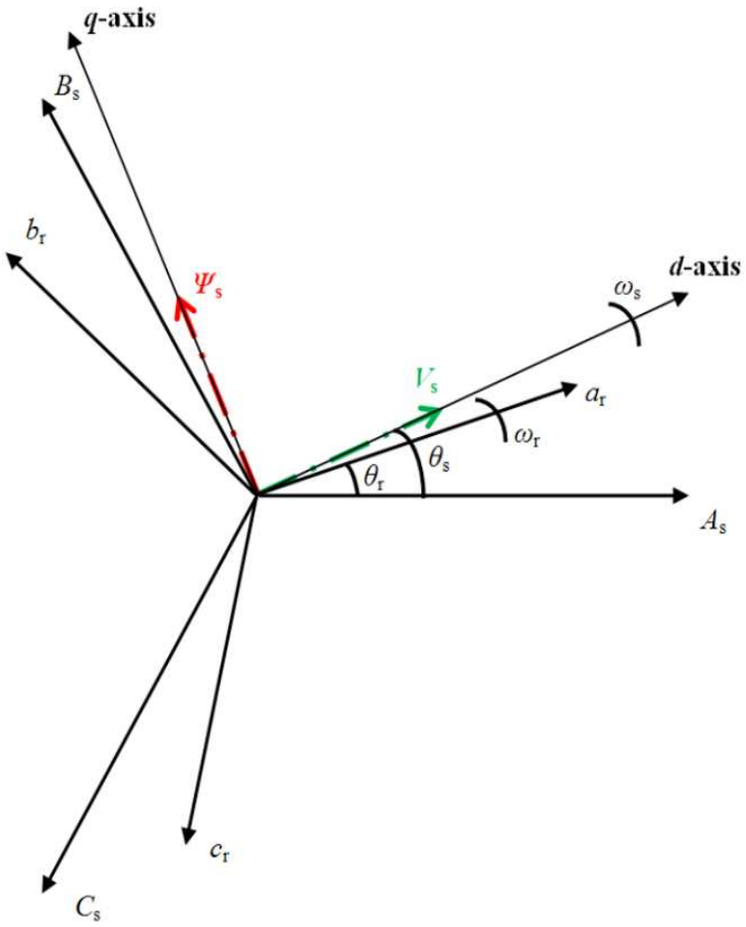

Figure 13. Stator voltage FOC reference frame

The V_{dr}^1 is called current regulation part and depicted by Figure 14, where $\sigma = L_r - L_m^2/L_s$. Due to the linear relationship between V_{dr}^1 and I_{dr}, the PI controller is employed. Besides, V_{dr}^2 is the cross-coupling part and requires feedforward compensation for a complete control. Eventually, the rotor-side converter voltage in *d*-axis is derived as:

$$V_{drc} = V_{dr} = V_{dr}^{1} + V_{dr}^{2} \tag{17}$$

where subscript rc denotes the rotor-side converter. After the conversion of *dq-abc*, the rotor-side converter voltage V_{abc_rc} can be obtained, which is used to generate PWM control signals for rotor-side converter.

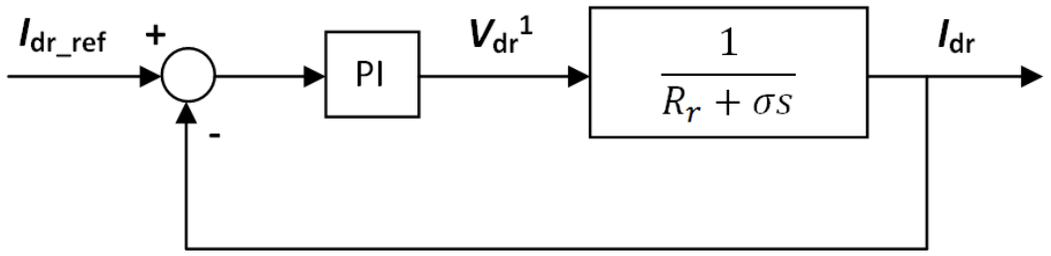

Figure 14. Current regulation part of *d*-axis rotor-side converter voltage

If only steady-state is considered, the derivative parts in Equation (10) are neglected and one can obtain stator flux as:

$$\begin{aligned} \Psi_{ds} &= \frac{V_{qs} - R_s I_{qs}}{\omega_s} \quad a \\ \Psi_{qs} &= \left(V_{ds} - R_s I_{ds}\right) / (-\omega_s) \quad b \\ \Psi_s &= \sqrt{\Psi_{ds}^2 + \Psi_{qs}^2} \quad c \end{aligned} \tag{18}$$

According to Equations (8), (10), and (12), the rotor-side converter reference current is derived as:

$$I_{dr\_ref} = -\frac{2L_s T_e}{3n_p L_m \Psi_s} \tag{19}$$

where

$$\begin{aligned} P_{e\_ref} &= P_{opt} - P_{loss} = T_e \omega_r \quad a \\ P_{loss} &= R_s I_s^2 + R_r I_r^2 + R_c I_{sc}^2 + F\omega_r^2 \quad b \end{aligned} \tag{20}$$

where I_{sc}, R_c, and F are stator-side converter current, choke resistance, and friction factor, respectively. P_{opt}, P_{e_ref}, and P_{loss} are desired optimal output active power, reference active

power, and system power loss, respectively. Combining Equations (8), (10), and (11), the active power is used as command inputs to determine current references I_{dr_ref}.

Similarly, the q-axis rotor-side converter voltage consists of current regulation and cross-coupling parts too:

$$\begin{aligned} V_{qr}^{\ 1} &= [R_r + \left(L_r - \frac{L_m^{\ 2}}{L_s}\right)\frac{d}{dt}]I_{qr} \quad a \\ V_{qr}^{\ 2} &= s\omega_s\left[L_r I_{dr} + L_m I_{ds} + \frac{L_m}{L_s}\frac{d\Psi_s}{dt}\right] b \end{aligned} \tag{21}$$

$$V_{qrc} = V_{qr} = V_{qr}^{\ 1} + V_{qr}^{\ 2} \tag{22}$$

where the derivative of stator flux in Equation (21b) is considered as zero at steady-state. Also, the current regulation part is illustrated in Figure 15. If the stator-side converter's reactive power is controlled to be zero, the output reactive power is stator reactive output power. Then, one has:

$$Q_o = Q_s + Q_{sc} = Q_s = = -V_{ds}I_{qs} = -V_{ds}\frac{1}{L_s}\left(\Psi_s - L_m I_{qr}\right) \tag{23}$$

Thus, the regulation of reactive power can lead to I_{qr_ref}.

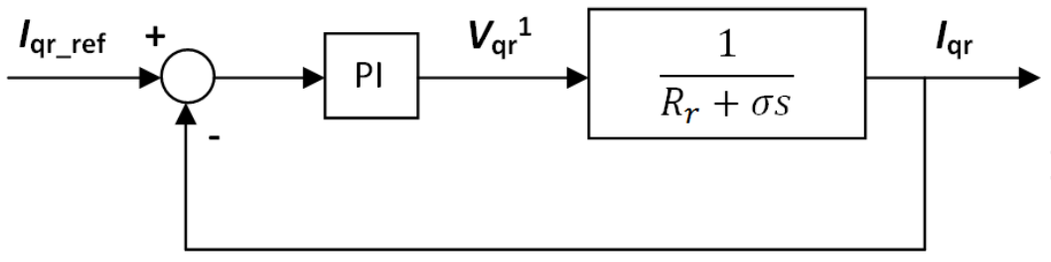

Figure 15. Current regulation part of q-axis rotor-side converter voltage

Involving the deviations of rotor voltage and reference currents in both d- and q-axis, Figure 16 exhibits the total control scheme for rotor-side converter, where the P_{opt} is obtained from MPPT.

2.3.3. Control of stator-side converter

The stator-side converter is controlled based on relationship between voltage, flux, and current of stator and choke, which is modeled by a cross-coupling model, as described in Figure 17. It

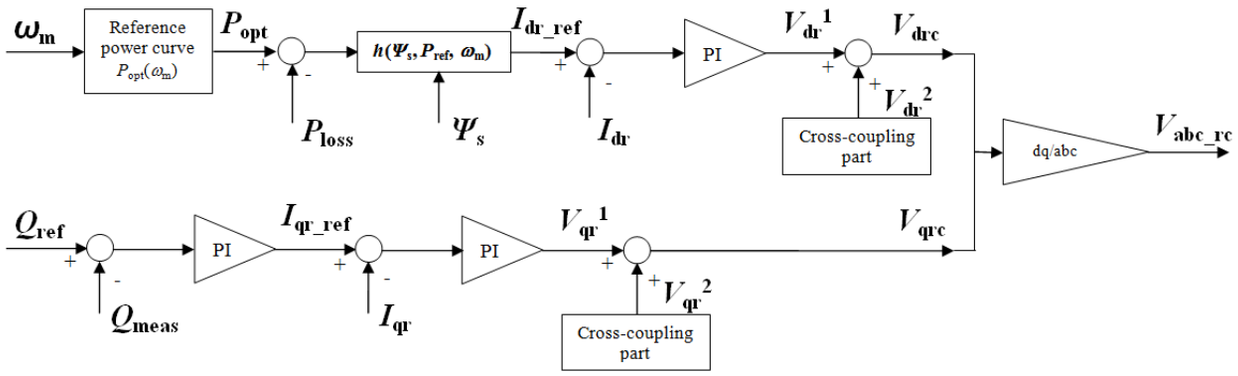

Figure 16. Total rotor-side converter control scheme

is seen that the grid (stator) voltage is equal to the sum of stator-side converter voltage and choke occupied voltage. By KVL:

$$\begin{aligned} V_{ds} &= R_c I_{dsc} - \omega_s \Psi_{qsc} + L_c \frac{dI_{dsc}}{dt} + V_{dsc}\, a \\ V_{qs} &= R_c I_{qsc} + \omega_s \Psi_{dsc} + L_c \frac{dI_{qsc}}{dt} + V_{qsc}\, b \end{aligned} \tag{24}$$

The flux linkage follows:

$$\begin{aligned} \Psi_{dsc} &= L_c I_{dsc}\, a \\ \Psi_{qsc} &= L_c I_{qsc}\, b \end{aligned} \tag{25}$$

Thus, the reorganized stator-side converter voltage in *d*- and *q*-axis, respectively, are presented as:

$$\begin{aligned} V_{dsc} &= V_{ds} - R_c I_{dsc} + \omega_s L_c I_{qsc} - L_c \frac{dI_{dsc}}{dt} a \\ V_{qsc} &= V_{qs} - R_c I_{qsc} - \omega_s L_c I_{dsc} - L_c \frac{dI_{qsc}}{dt} b \end{aligned} \tag{26}$$

where the subscripts sc and ch denote the variables of stator-side converter and choke, respectively. L_c and R_c are the inductance and resistance of the choke.

Based on the model in Equation (26a, b), the current regulation part of choke voltage in *d*- and *q*-axis are described as (27a, b) and Figure 18(a, b).

http://dx.doi.org/10.5772/60958

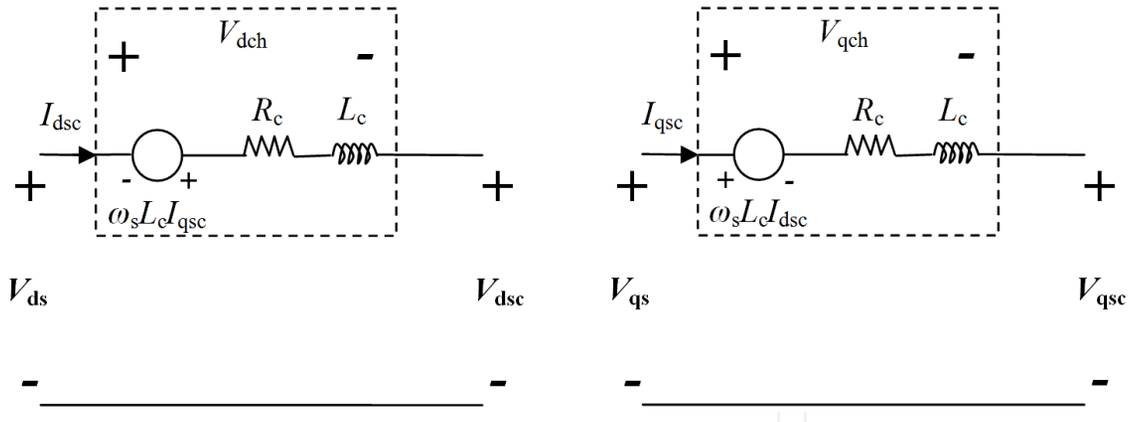

Figure 17. Equivalent circuit of stator-side converter choke [23]

$$V_{dch}{}^{1} = \left(R_c + L_c \frac{d}{dt} \right) I_{dsc}\, a$$
$$V_{qch}{}^{1} = \left(R_c + L_c \frac{d}{dt} \right) I_{qsc}\, b \tag{27}$$

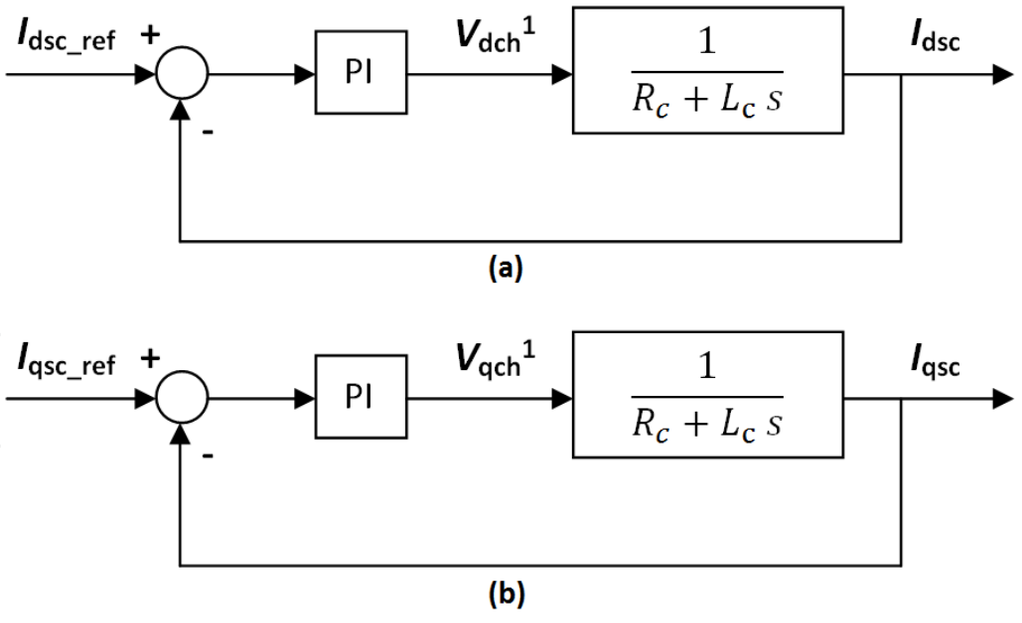

Figure 18. Current regulation part of choke voltage ((a) *d*-axis; (b) *q*-axis)

The cross-coupling part of choke voltage V_{dch2} and V_{qch2} are expressed as (28a, b) and the total stator-side converter voltage is derived as (29a, b).

$$V_{dch}{}^{2} = -\omega_s L_c I_{qsc} \quad a$$
$$V_{qch}{}^{2} = \omega_s L_c I_{dsc} \quad b \tag{28}$$

$$V_{dsc} = V_{ds} - V_{dch}{}^{1} - V_{dch}{}^{2} \quad a$$
$$V_{qsc} = V_{qs} - V_{qch}{}^{1} - V_{qch}{}^{2} \quad b \tag{29}$$

The current reference I_{qsc_ref} is generally set at zero for zero reactive power output from stator-side converter while I_{dsc_ref} is determined by the regulation of dc-link voltage V_{dc}. The stator-side converter voltage control is depicted in Figure 19.

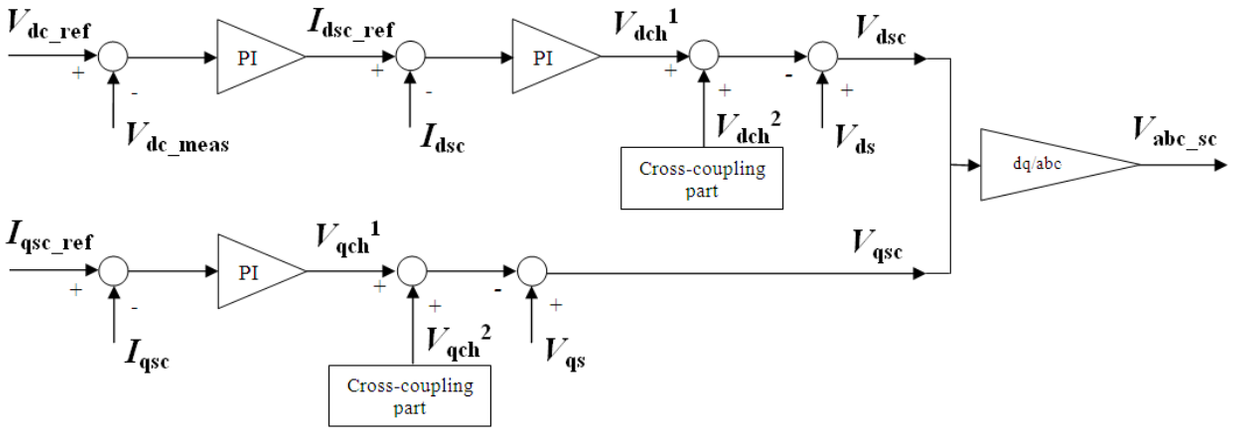

Figure 19. Total stator-side converter control scheme [23]

With both rotor- and stator-side converter controls, the simulation results [23] in Figure 20 present a stable and controllable dynamic response to a gusty wind speed. Also, an FRT capability is verified by a voltage droop happening within a constant wind speed. Figure 21 shows twice oscillations at two dynamic moments and the control system effectively recovers the system-regulated outputs in short amount of time.

2.3.4. Space Vector Modulation (SVM)

The purpose of both rotor- and stator-side converter controls is to obtain the reference voltages which are expected to be produced by the converter. The next step is obviously to generate the corresponding PWM gate signals for the converter. To a 2-level three-phase voltage source inverter, there are six switches of three legs in inverter controlling the phase voltage and thus the current of induction generator. By defining the “ON” and "OFF" states of upper switch by “1” and “0,” respectively, for one leg, there exist up to eight different states for inverter outputs. They are summarized in Table 2 as well as the resulted phase voltage in *abc* and $\alpha\beta$ frames. Eight inverter output voltages can be considered as eight voltage vectors [0, 0, 0] through [1, 1, 1] that are illustrated in Figure 22.

http://dx.doi.org/10.5772/60958

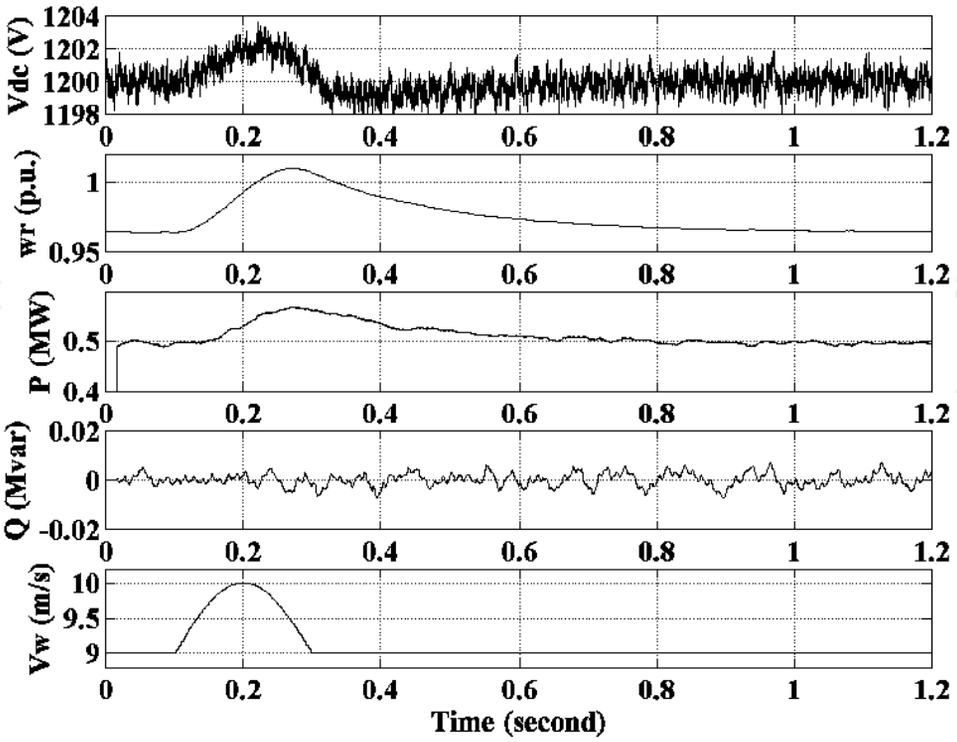

Figure 20. Gusty wind responses ((a) DC-link voltage V_{dc}; (b) generator speed ω_r; (c) active power P; (d) reactive power Q; (e) wind speed V_w)

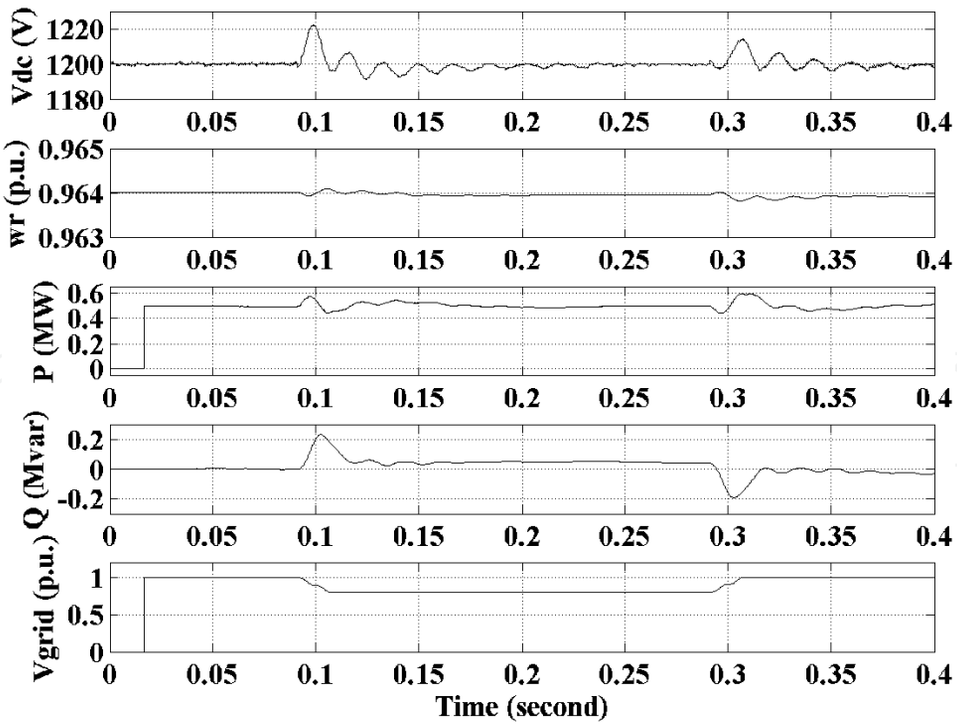

Figure 21. Dynamic responses to grid voltage droop ((a) DC-link voltage V_{dc}; (b) generator speed ω_r; (c) active power P; (d) reactive power Q; (e) grid voltage V_{grid})

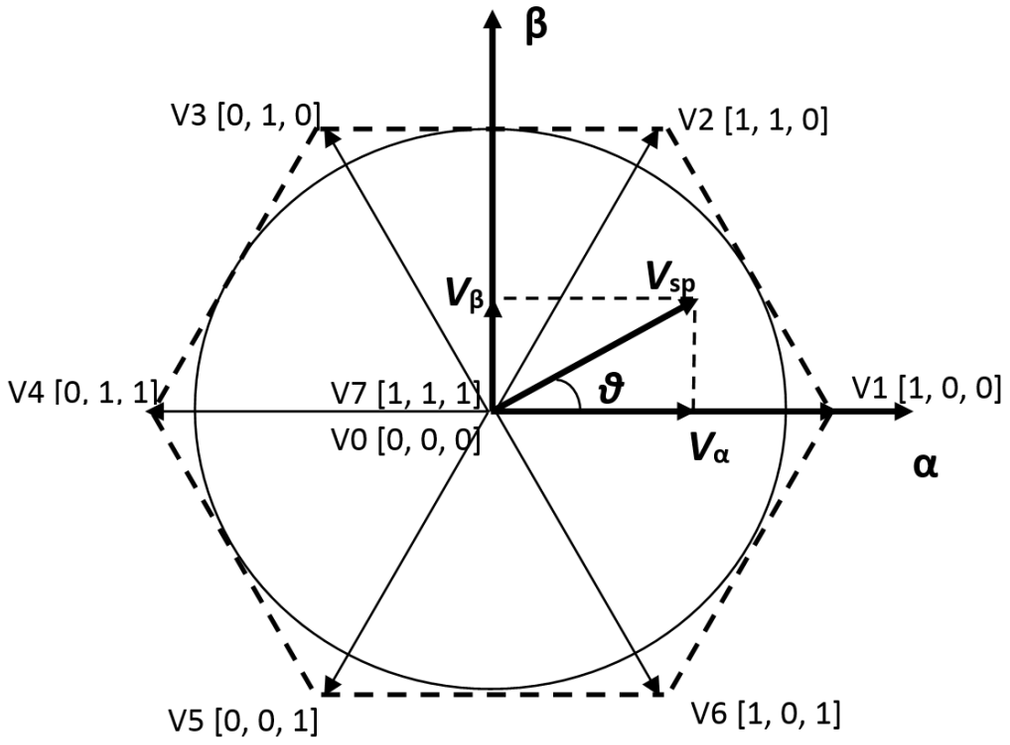

Figure 22. Eight inverter voltage space vectors

L_1	L_2	L_3	V_{an}	V_{bn}	V_{cn}	V_α	V_β
1	1	1	0	0	0	0	0
1	0	0	$2V_{dc}/3$	$-V_{dc}/3$	$-V_{dc}/3$	$\sqrt{(2/3)}V_{dc}$	0
1	1	0	$V_{dc}/3$	$V_{dc}/3$	$-2V_{dc}/3$	$\sqrt{(1/6)}V_{dc}$	$\sqrt{(1/2)}V_{dc}$
0	1	0	$-V_{dc}/3$	$2V_{dc}/3$	$-V_{dc}/3$	$-\sqrt{(1/6)}V_{dc}$	$\sqrt{(1/2)}V_{dc}$
0	1	1	$-2V_{dc}/3$	$V_{dc}/3$	$V_{dc}/3$	$-\sqrt{(2/3)}V_{dc}$	0
0	0	1	$-V_{dc}/3$	$-V_{dc}/3$	$2V_{dc}/3$	$-\sqrt{(1/6)}V_{dc}$	$-\sqrt{(1/2)}V_{dc}$
1	0	1	$V_{dc}/3$	$-2V_{dc}/3$	$V_{dc}/3$	$\sqrt{(1/6)}V_{dc}$	$-\sqrt{(1/2)}V_{dc}$
0	0	0	0	0	0	0	0

Table 2. Space vector states (L_1–L_3 represent inverter leg1–leg3)

Once the reference space vector voltage in $\alpha\beta$ frame is achieved by current regulation, the magnitude and angle of the voltage are used to implement the SVM. With constant PWM frequency, a space vector is always realized by a vector sum of two adjacent vectors in Table 2. Taking the space vector voltage (0 to 60 degree section) in Figure 23 as an example, it is equal to the vector sum of V_1 and V_2 with magnitudes of d_x and d_y, respectively, which are the duty cycles of two vectors [32]:

http://dx.doi.org/10.5772/60958

$$d_x = \frac{|V_{sp}|}{\sqrt{\frac{2}{3}}V_{dc}} \frac{\sin\left(60^\circ - \gamma\right)}{\sin 60^\circ} a$$
$$d_y = \frac{|V_{sp}|}{\sqrt{\frac{2}{3}}V_{dc}} \frac{\sin\gamma}{\sin 60^\circ} \quad b \tag{30}$$
$$d_z = 1 - d_x - d_y \quad c$$

where d_z denotes the duty cycle of zero vector. Generally, the zero vectors [0, 0, 0] or [1, 1, 1] contribute the remaining PWM period after d_x and d_y. The space vector voltages located in other sections can follow the same procedure to obtain the duty cycles of d_x, d_y, and d_z. Then, the Minimum-Loss Space Vector PWM (MLSVPWM) technique is applied to determine the sequence of vectors [32]. The PWM signals are eventually obtained based on computed duty cycles and sequence of vectors. Figures 24 and 25 show the simulation and experimental three-phase duty ratios for inverter phase A, B, and C, where no switching action happens if 0 or 1 duty cycle is the case. It is seen that there is always one phase being absent of switching at any moment, which minimizes the switching loss of the semiconductor switches. Also, the experimental results reveal the sinusoidal nature of the line voltage duty ratio that is expected for sinusoidal fundamental line voltage output of inverter. With this PWM SVM technique, the rotor- and stator-side converters are controlled by previously derived FOC.

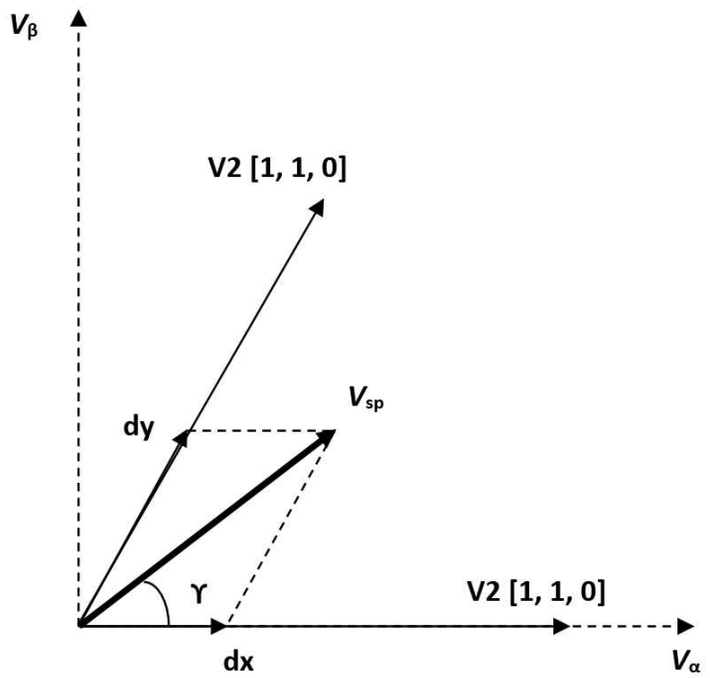

Figure 23. Duty cycles of vectors for reference space vector voltage

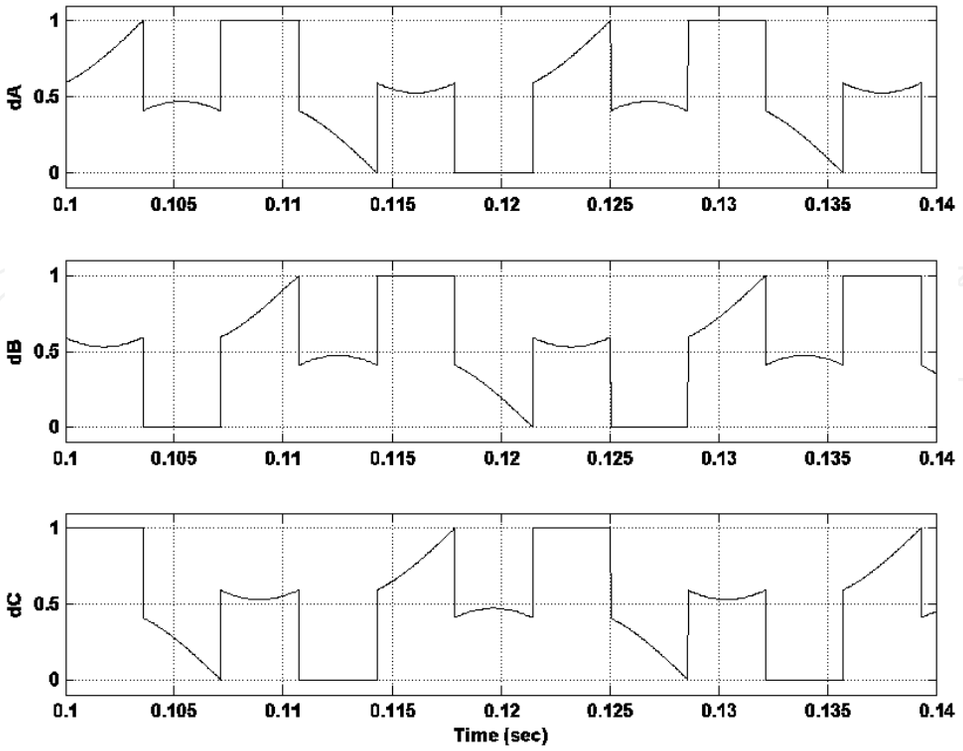

Figure 24. Three-phase duty cycles using MLSVPWM (simulation results [33])

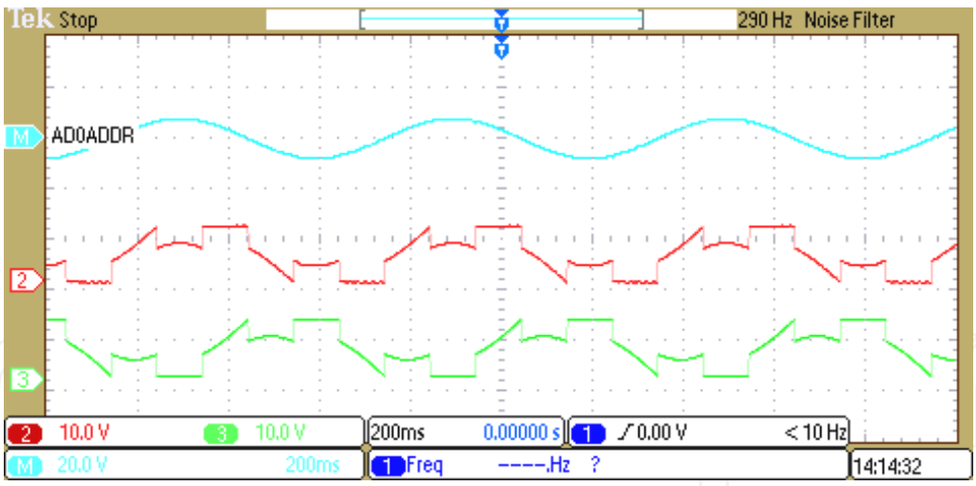

Figure 25. Phase duty cycles and phase-to-phase duty cycle using MLSVPWM (experiment results [33])

2.3.5. Islanded operation

Compared to the grid integration DFIG wind system, the isolated DFIG wind system operating at regulated voltage (magnitude and frequency) is also found applicable and valuable to some independent power subgrid or distributed power systems. One of the application examples – DFIG-Synchronous machine system configuration – is shown in

http://dx.doi.org/10.5772/60958

Figure 26. Modified FOC for power generation in Figure 27 is used and the line voltage magnitude and frequency are stabilized by extra variable load and synchronous machine. The line frequency is held by compensating the resistive load, while the line voltage is held by feeding controlled field voltage of synchronous machine. The proposed controller scheme in [34] is employed for synchronous machine field voltage controller. As shown in Figure 28(a, b), the line frequency is regulated at 60Hz with limited error while the line voltage is regulated at 1 p.u. The constant frequency and magnitude in transmission line voltage is the basic requirement for a controllable power delivery. Based on the regulations of frequency and line voltage, the active power and reactive power are also under controlled respectively [25]. The dc-link voltage is kept at nominal value, while the generator speed is controlled at optimal 0.95 p.u., as shown in Figure 29.

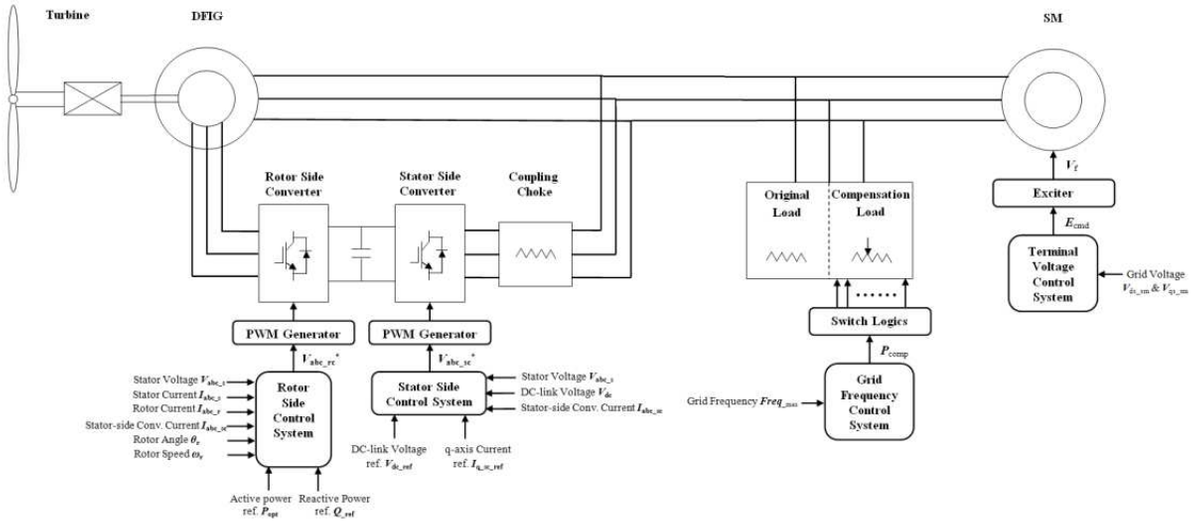

Figure 26. Islanded DFIG-Synchronous machine wind power system

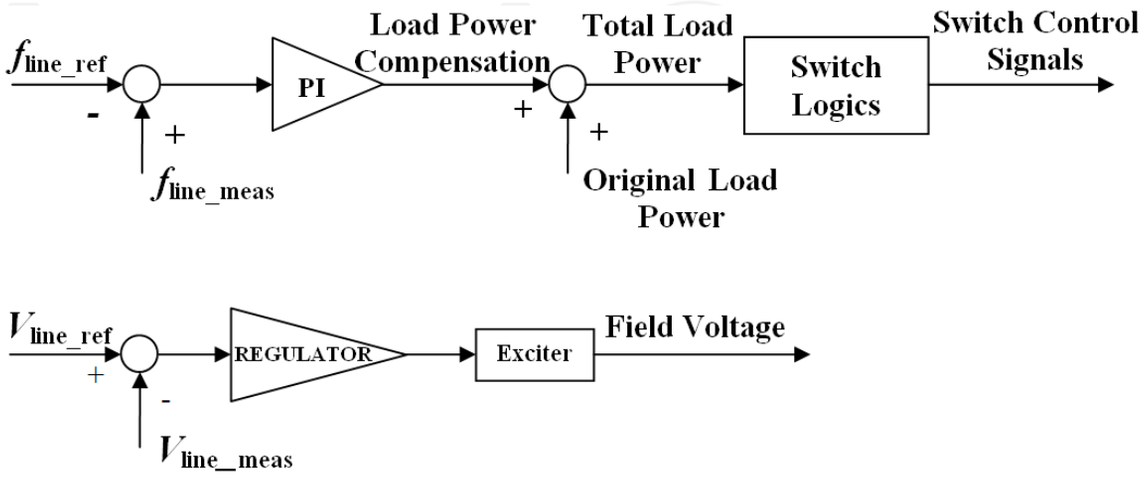

Figure 27. DFIG-Synchronous machine system control scheme

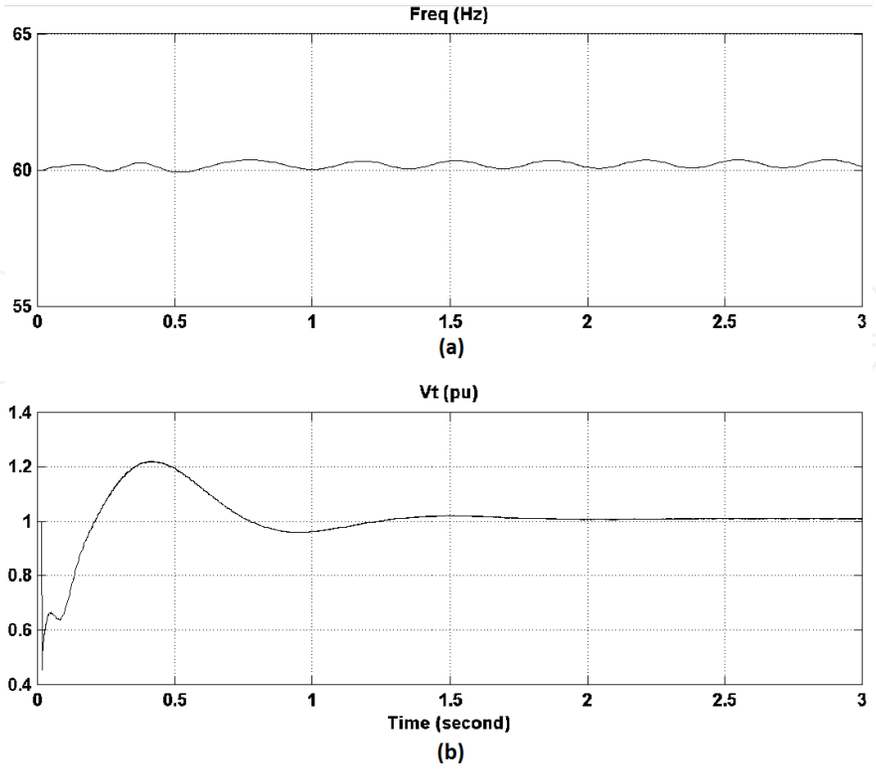

Figure 28. Line voltage and frequency in islanded DFIG system ((a) line frequency; (b) line voltage)

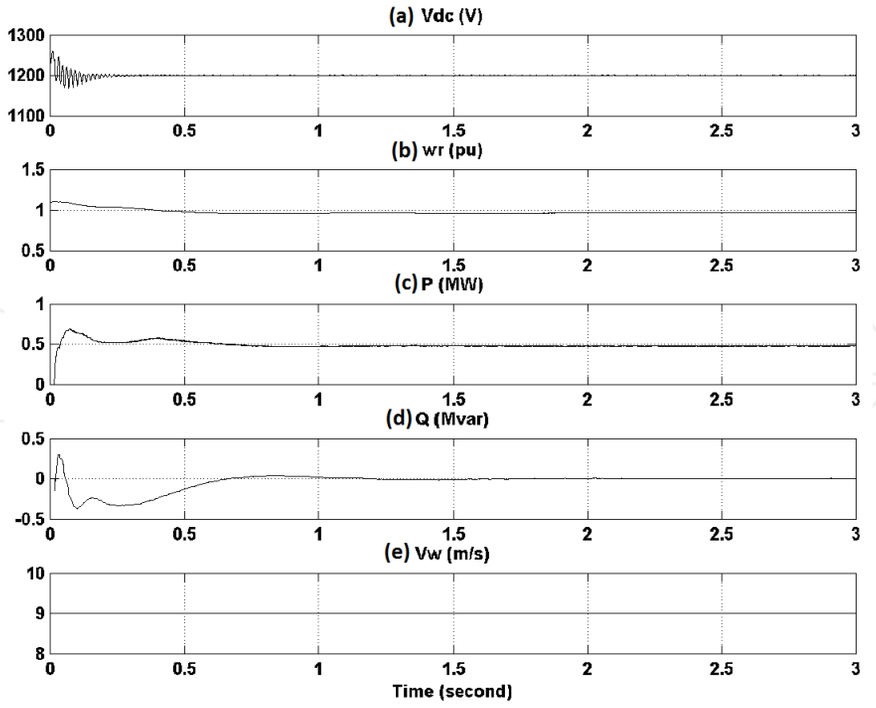

Figure 29. Simulation results for islanded operation ((a) dc-link voltage V_{dc}; (b) generator speed ω_r; (c) active power P; (d) reactive power Q; (e) wind speed V_w)

2.4. Grid synchronization

The key to performing FOC is to follow the position angle of the *d*-axis component so that the output can be synchronized with *dq* frame, especially in the grid integration operation mode. In order to operate in this mode, the induction generator voltage must be synchronized with the grid voltage by applying the Phase Lock Loop (PLL) technique. The technique takes the grid signal as input and keeps track of the position angle of the grid voltage for FOC as well as reproducing the grid voltage frequency as output, in a real-time manner. To introduce the algorithm, assume an estimated grid voltage angle (accurate grid voltage angle of θ); the resulting grid voltages in *dq* frame are written as:

$$\begin{aligned} V_d &= V_\alpha \cos\hat{\theta} + V_\beta \sin\hat{\theta}\, a \\ V_q &= -V_\alpha \sin\hat{\theta} + V_\beta \cos\hat{\theta} b \end{aligned} \tag{31}$$

where

$$\begin{aligned} V_\alpha &= V_m \cos\theta\, a \\ V_\beta &= V_m \sin\theta\, b \end{aligned} \tag{32}$$

and V_m denotes the magnitude of the voltage space vector. By substituting V_α and V_β in (31a, b) by (32a, b), the V_d and V_q can be organized as:

$$\begin{aligned} V_d &= V_m \cos\left(\theta - \hat{\theta}\right) a \\ V_q &= V_m \sin(\theta - \hat{\theta}) b \end{aligned} \tag{33}$$

It is seen that if is equal to θ, V_d is equal to V_m, and V_q is equal to 0. Therefore, the accurate grid voltage angle θ can be obtained by regulating the grid voltage V_q to zero. Assuming there is an error δ between and θ that $\delta = \theta -$, due to the small value of δ, it is true that $V_q \cong V_m\delta$ and the PLL system in s-domain can be described as Figure 30, where (s) denotes the estimated grid voltage angular frequency and $K_c(s)$ is a PI controller. After removing the unknown accurate θ, the PLL scheme is essentially a regulation of V_q in Figure 31, where the measured V_q goes through a 1st-order low-pass filter whose cutoff frequency is ω_c. In this way, the noise is effectively eliminated.

The introduced PLL algorithm is simulated and shown in Figure 32, as well as zoom-in image in Figure 33 [33], where 0 radian grid voltage position coincides with the zero-crossing of phase voltage V_{an} and the frequency can be detected to be 60Hz after short transient (the initial grid frequency is assumed as 55Hz). These results indicate a successful "locking" of grid frequency and position angle, with which the FOC (Figures 16 and 19) are conducted on back-to-back converter in a real-time manner and can thus continuously "match" the generated voltage with the grid voltage.

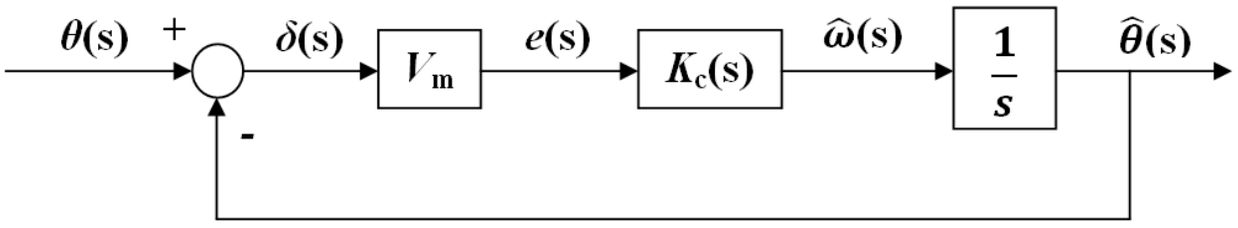

Figure 30. PLL scheme for grid voltage angle estimation

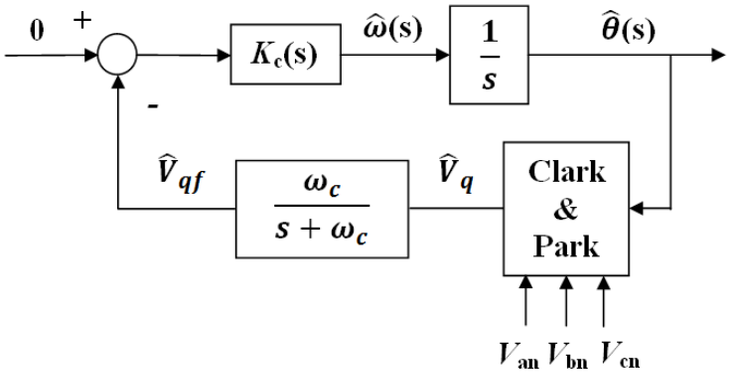

Figure 31. PLL scheme with regulation of V_q

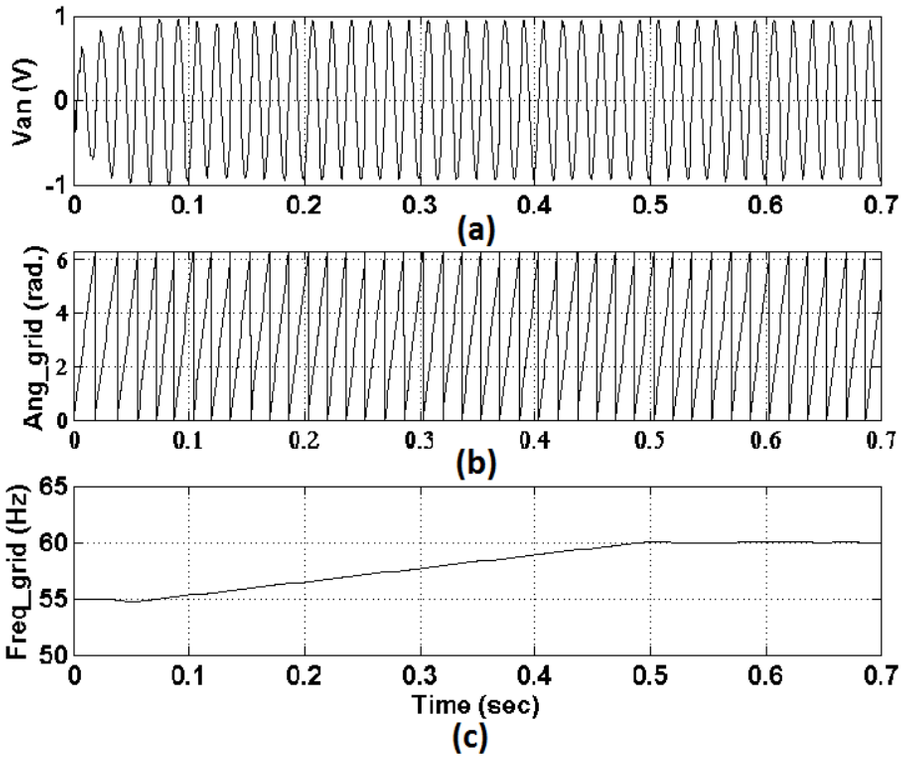

Figure 32. PLL results of grid voltage angle and frequency for grid integration operation ((a) phase A voltage V_{an}; (b) grid voltage angular position; (c) grid voltage frequency)

http://dx.doi.org/10.5772/60958

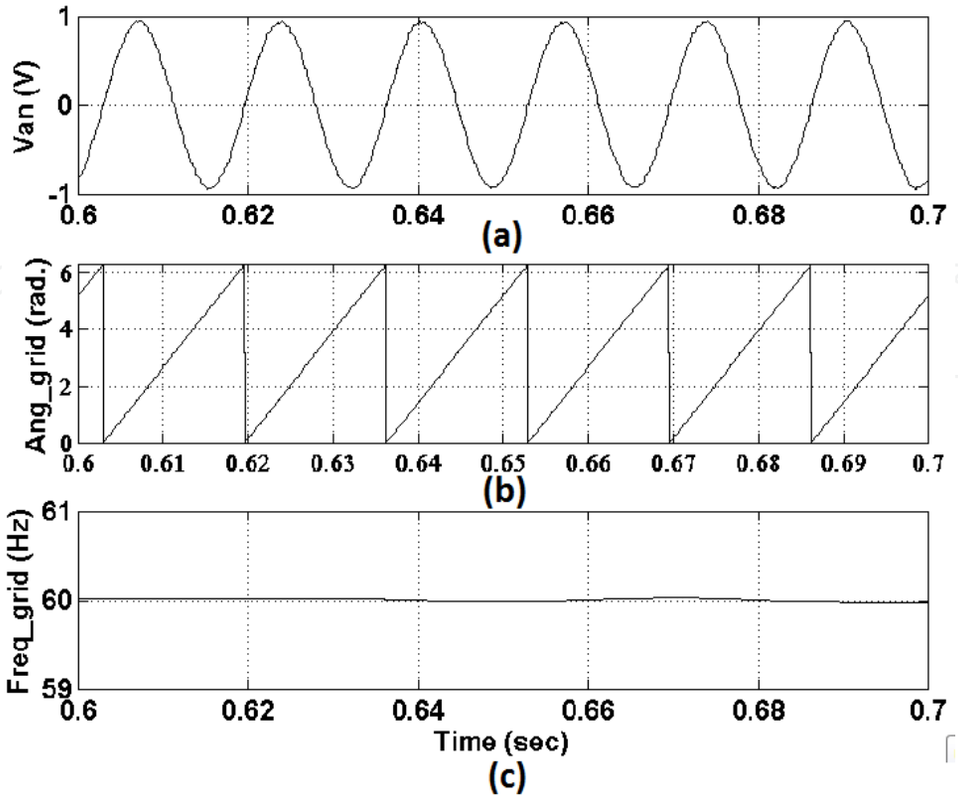

Figure 33. Zoom-in image of Figure 32

3. Maximum Power Point Tracking (MPPT)

Efficiency always plays an important role in induction generator wind systems. While the SCIG system loses precise control of power due to the fixed-speed operation, to achieve high efficiency in wind power conversion systems, the MPPT in variable-speed DFIG system has been intensively investigated. Basically, the studied techniques in MPPT include three strategies: (1) the methods relying on wind speed, (2) the methods relying on output power measurement and calculation, and (3) the methods relying on reference power curve.

3.1. Pitch angle control of induction generator wind systems

An overall picture of induction generator wind system operation versus wind speed is depicted in Figure 34, where the output power must be "truncated" after reaching certain level. Pitch angle control, as investigated in section 2.2, is used not only in SCIG system but also in DFIG system for this purpose. It is seen that the capability of pitch angle control in response to the increase of wind speed, on limiting the power output, is primarily dependent on turbine blade physical structure. Therefore, the system needs to be shut down by brake system in the case of wind speed cutoff. Figure 34 also emphasizes the augmented power output of MPPT operation over fixed-speed operation and this inspires the investigation of advanced variable-

speed wind systems, where the induction generator speed can always be controlled in a large range to capture desired output power by combining the previously discussed FOC with MPPT strategies.

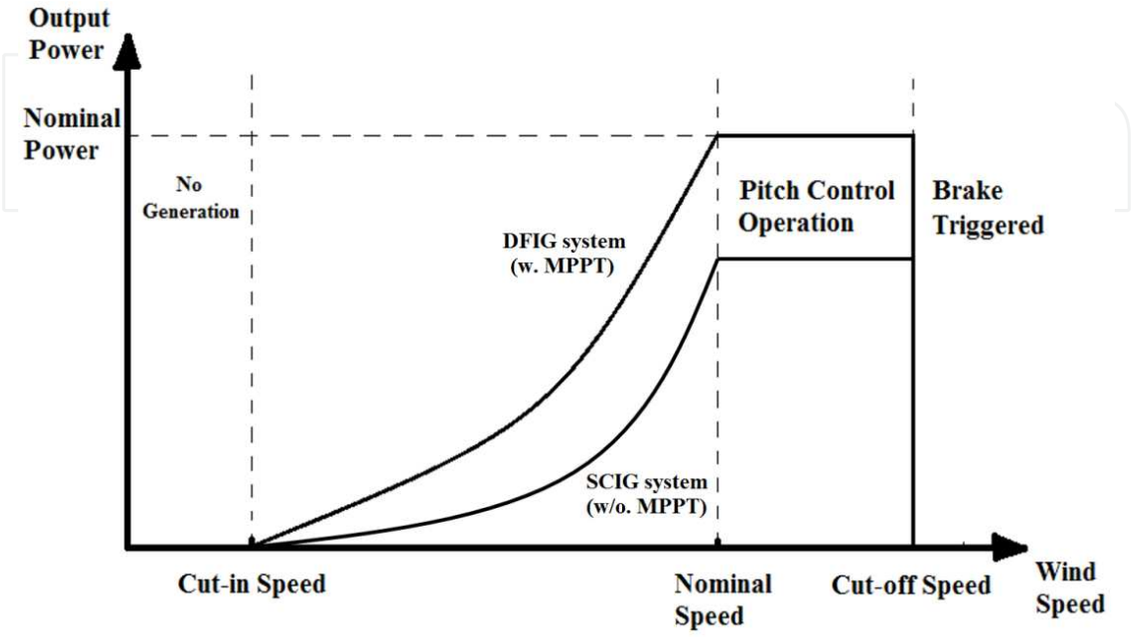

Figure 34. Wind power system operations

3.2. MPPT methods for DFIG wind systems

3.2.1. Wind speed based method

Most DFIG wind power systems are dependent of wind speed measurement [2,4]. In these systems, anemometers are applied to measure the wind speed and thus the systems suffer from additional cost of sensors and complexity. In order to solve this problem, wind speed estimation methods have been reported [25, 35-36]. Relying on the complex algorithms, the accurate wind speed can be captured for controlling the optimal tip speed ratio so that the MPPT can be performed accordingly, as shown in Figure 35. However, the wind speed information and associated efforts on software/hardware are still necessary and significant. To eliminate the dependence on wind speed, some sensorless control strategies have been developed [31,37-38]. These methods are in test for small-scale stand-alone systems and the complicated estimation algorithms remain, which will result in weakening of accuracy and control speed in real operating environment where the wind speed changes rapidly.

3.2.2. Power variation rate based method

Tracking the maximum power can also be accomplished through measuring the output power directly [39-42]. The idea of this method is through checking the variation rate of the output power with respect to that of generator speed ($dP/d\omega$), the power operation point location can

http://dx.doi.org/10.5772/60958

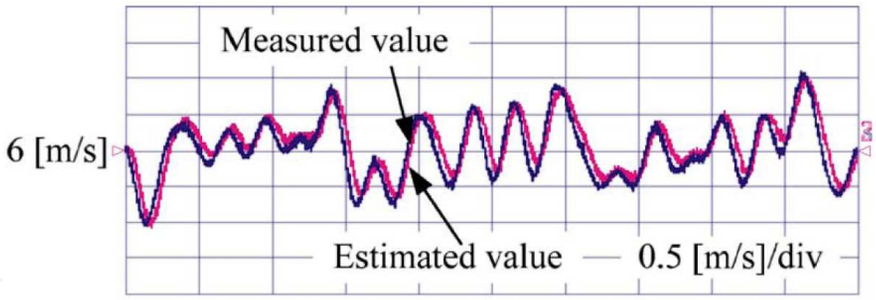

Figure 35. Estimated wind speed and real measured wind speed [35]

be determined and be accordingly controlled thereafter. Theoretically, the maximum power operating point can be reached when $dP/d\omega = 0$, as shown in Figure 36. A flowchart of the algorithm is shown in Figure 37, where the operation point (ω_m (k), P(k)) is measured and compared with (ω_m(k-1), P(k-1)) under wind speed V_w(i), where i is the index of wind speed; k is given as the test step index under particular wind speed V_w(i). Among all the tested points, only one point holds the truth that $dP/d\omega = 0$ and it is the optimal operation point (ω_{mopt}(i), P_{opt}(i)) that will be returned and saved. This procedure is required in a means of real-time for different wind speed (i=1,2,...,). According to the information from the optimal points, either the generator speed or the duty cycle of converter can be tuned.

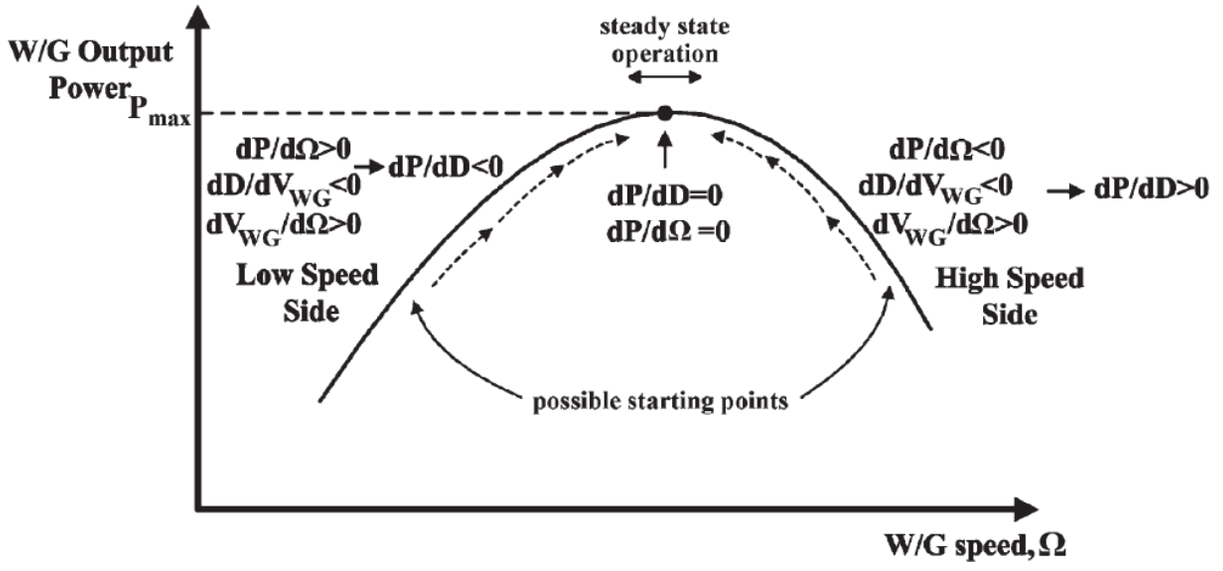

Figure 36. MPPT based on output power varying rate [41]

3.2.3. Reference power curve based method

Besides the above strategies, MPPT can be carried out by means of tracking the reference (optimal) power curve, which is the fitting curve going through all the maximum power points of all wind speeds [43-45]. A generalized reference power curve is given as:

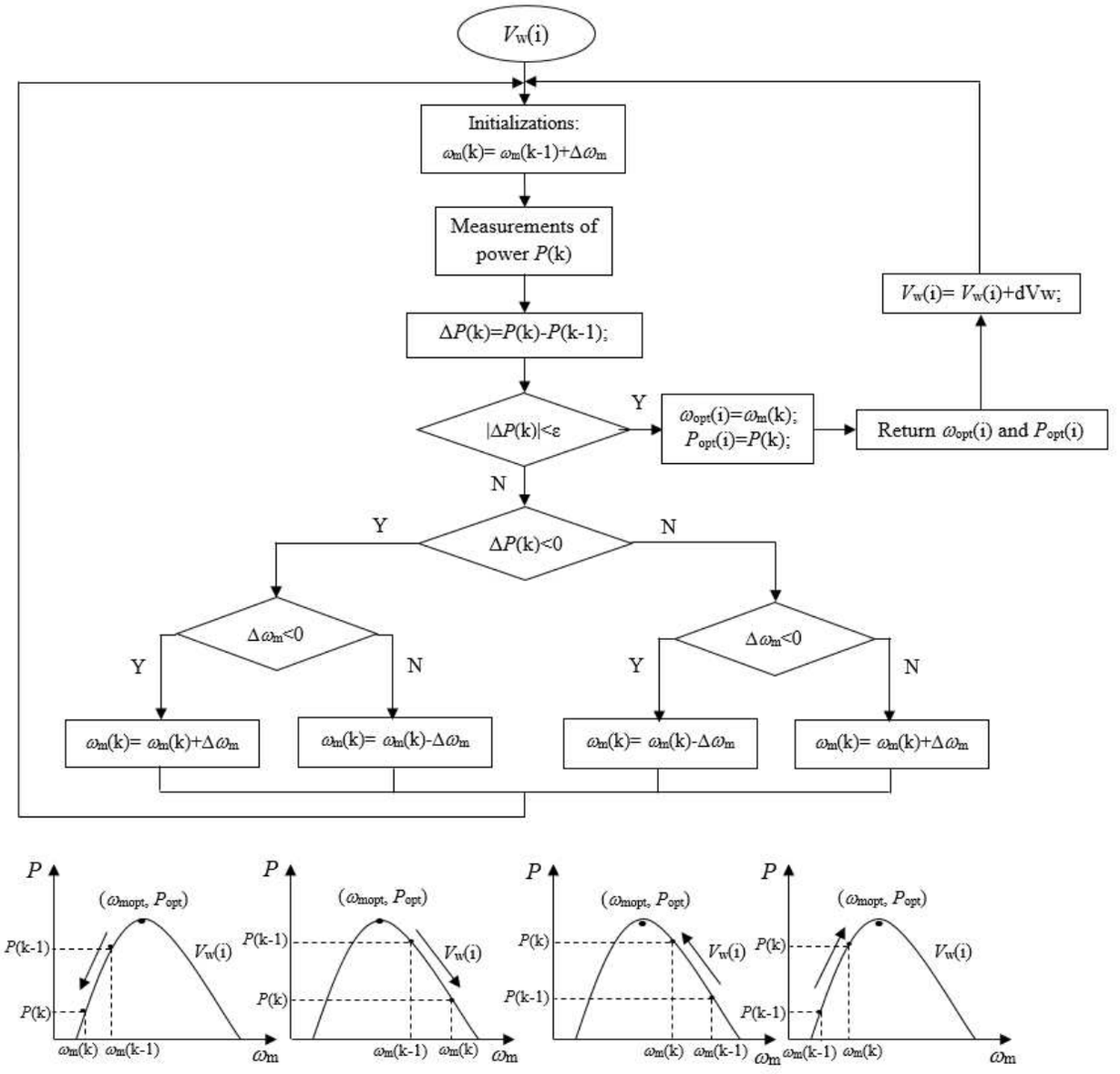

Figure 37. Flow chart of power variation rate testing algorithm

$$P_e = b_k \omega_m^k + b_{k-1} \omega_m^{k-1} + \ldots + b_1 \omega_m + b_0 \tag{34}$$

To determine the optimal degree of the polynomial, comparison is conducted for a 2.678 MW DFIG wind system [33]. Under a particular wind speed, four reference curves lead to four different operation points and the 3rd-order polynomial in Equation (35) leads to the most accurate reference curve along optimal operation points, as shown in Figure 38.

$$P_e = b_3 \omega_m^3 + b_2 \omega_m^2 + b_1 \omega_m + b_0 \tag{35}$$

http://dx.doi.org/10.5772/60958

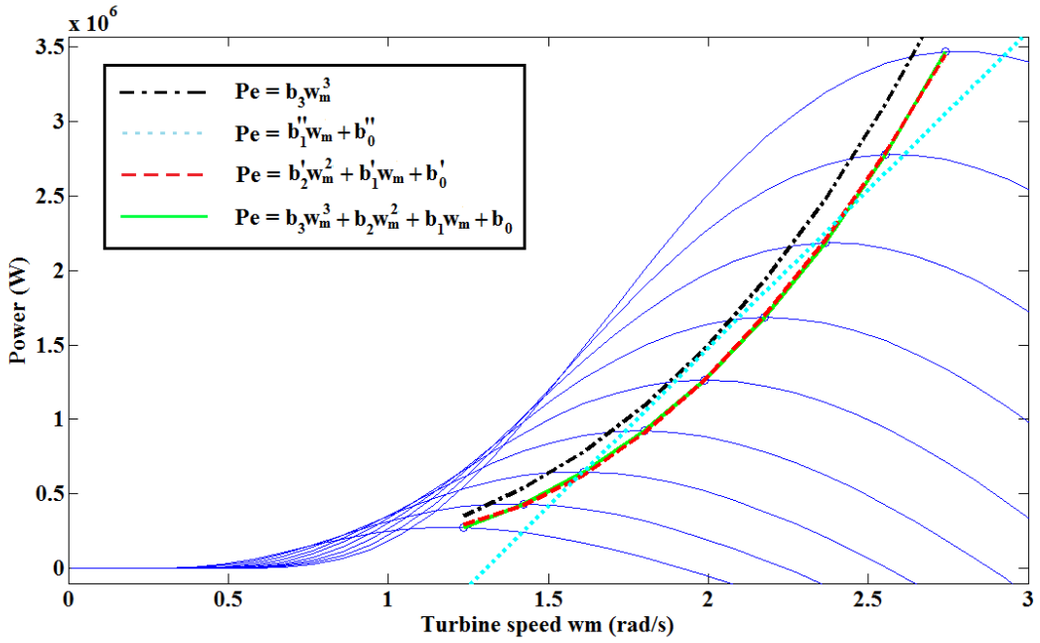

Figure 38. Comparison of reference power curve fittings

This method has been widely used due to its simple concept and absence of extra wind measurement costs. The optimal reference power curve is constructed according to the experimental tests and programmed in a microcontroller memory, to be used as a lookup table. The algorithm diagram is illustrated in Figure 39. Either the generator speed is measured to obtain power reference for power regulation, or the wind speed is measured to obtain generator speed reference for generator speed regulation. The former method produces more accurate output power, while the latter has faster control speed [25]. Some research works simply apply a cube function of generator speed as reference power or a square function of generator speed as reference torque. Despite these feasible solutions, the accurate maximum power and corresponding optimal generator speed are undervalued. Such approximation will obviously lead to harmed power generation efficiency. More importantly, analysis is necessary to verify the stability of the method in terms of varying wind speed and output power.

An evolved solution was proposed in [47] to effectively minimize the drawback of the above method. The real-time tuning of reference power curve coefficients is conducted and followed by updating the reference power curve. First, instead of disturbing output power directly, the most significant coefficient is incrementally disturbed by constant. This change of reference power curve induces the variation of the output power, which is measured and compared with previous step power. When the difference in output power between two consecutive steps approaches a small enough value, the disturbed coefficient is returned to update the reference power curve. The resulting reference power curve is the accurate optimal reference power curve. Due to the existence of reference power curve, such tuning

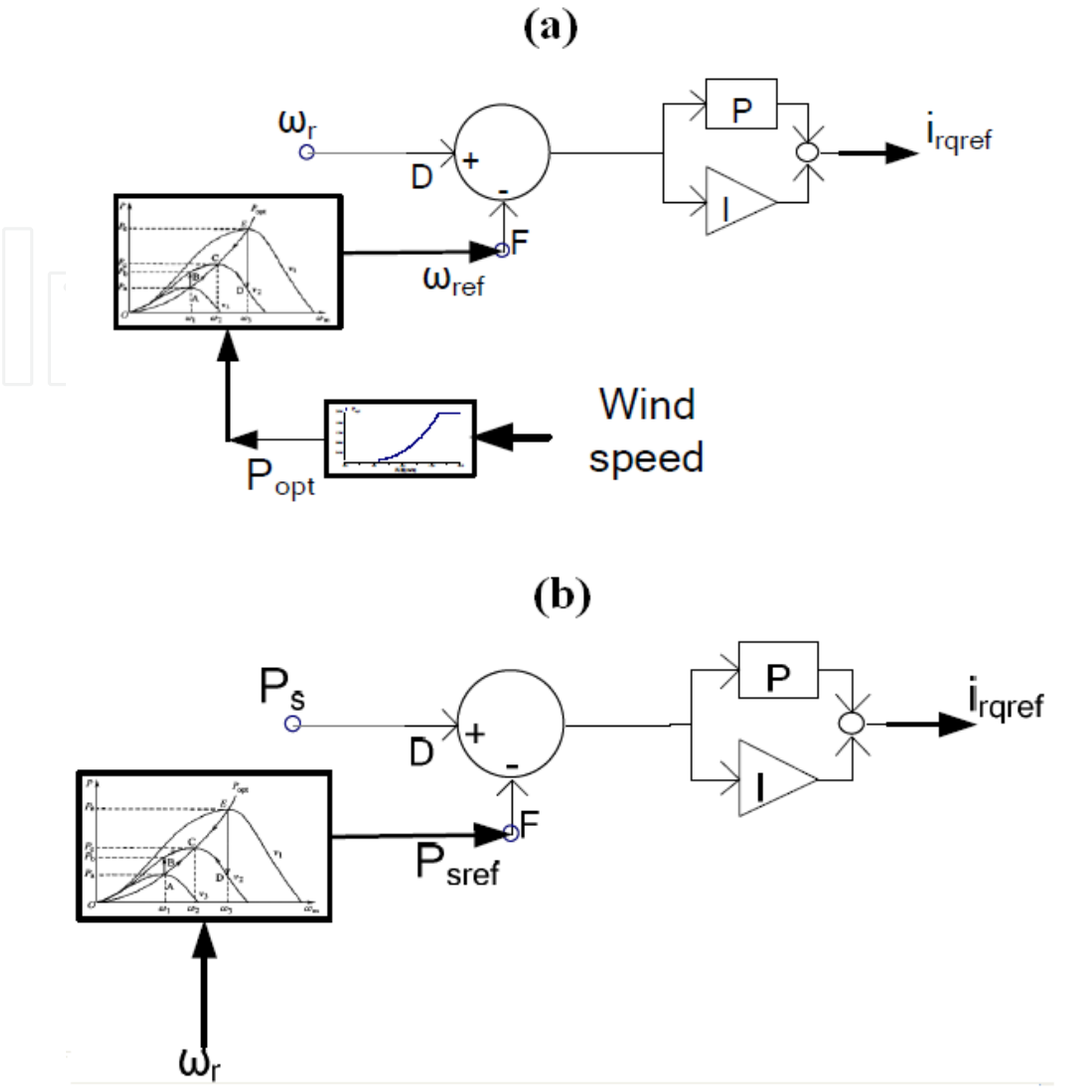

Figure 39. MPPT based on reference power curve [46]

calculation does not need to be conducted continuously with high frequency. In addition, without disturbing output power directly, this method can conduct updating and perturbation faster. Moreover, any deviation of system model will not give rise to deviation of optimal power generation because of the real-time tuning. Thus, the method is robust. As depicted in Figure 40, power variation is checked to capture the optimal coefficient and the reference power curve is updated accordingly to lead the system running in MPPT mode. The whole procedure is described in the simulation results in Figures 41 and 42, where the perturbation of coefficient b_3, the generator speed, and generated power halt after reaching the optimal values. No more perturbation and updating are needed, thus saving the calculation cost. Despite the oscillations at each b_3 perturbation step, the dc-link voltage and the reactive power remain at desired values while the output power and generator speed are updated, step by step, toward the optimal values. The generator speed and output power are generally measured with much higher frequency than that of perturbation. It is

http://dx.doi.org/10.5772/60958

also worth noting that the bandwidth of b_3 updating must ensure that both generator speed and output power are able to reach their steady-states.

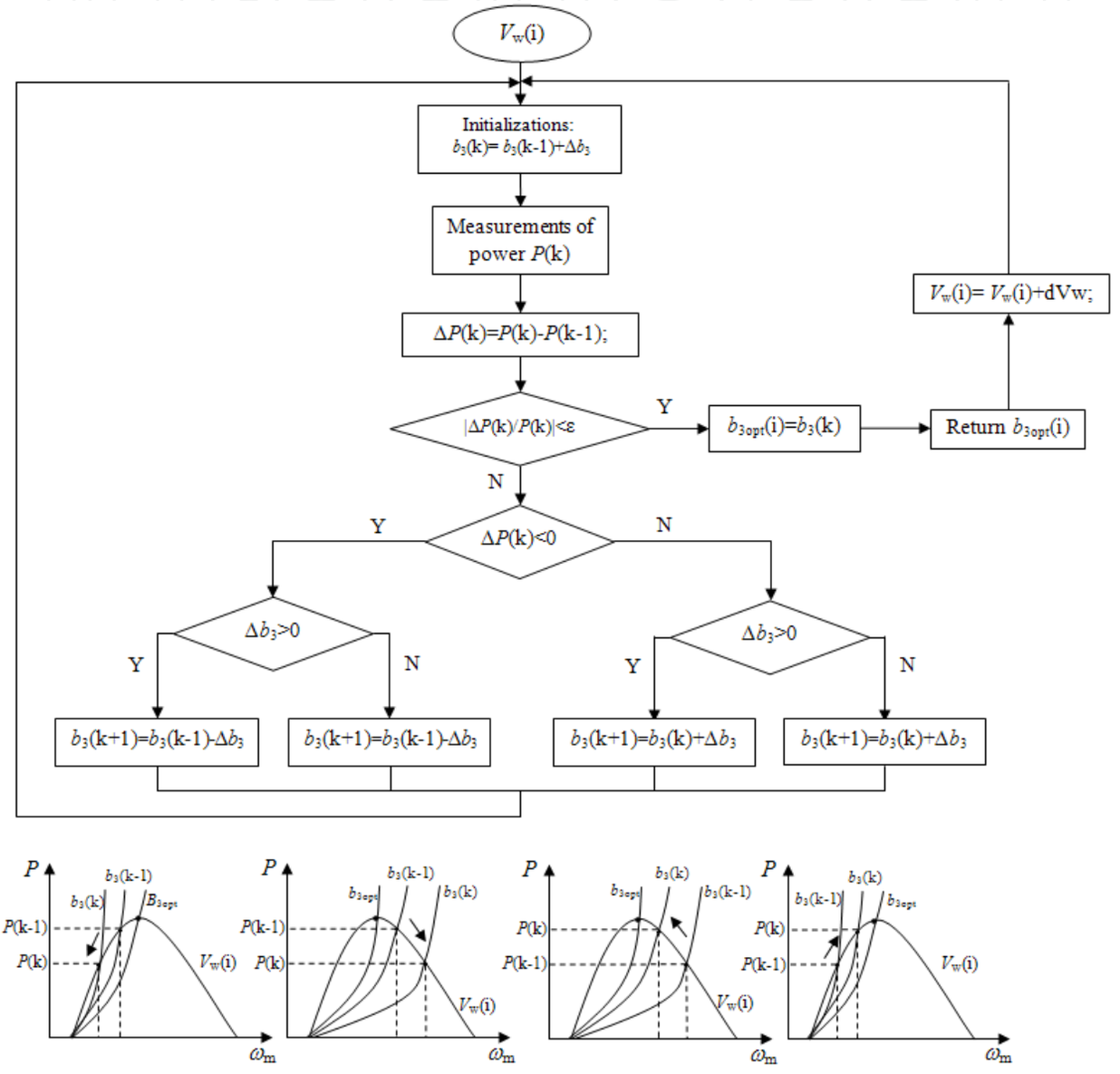

Figure 40. Novel MPPT algorithm proposed in [47]

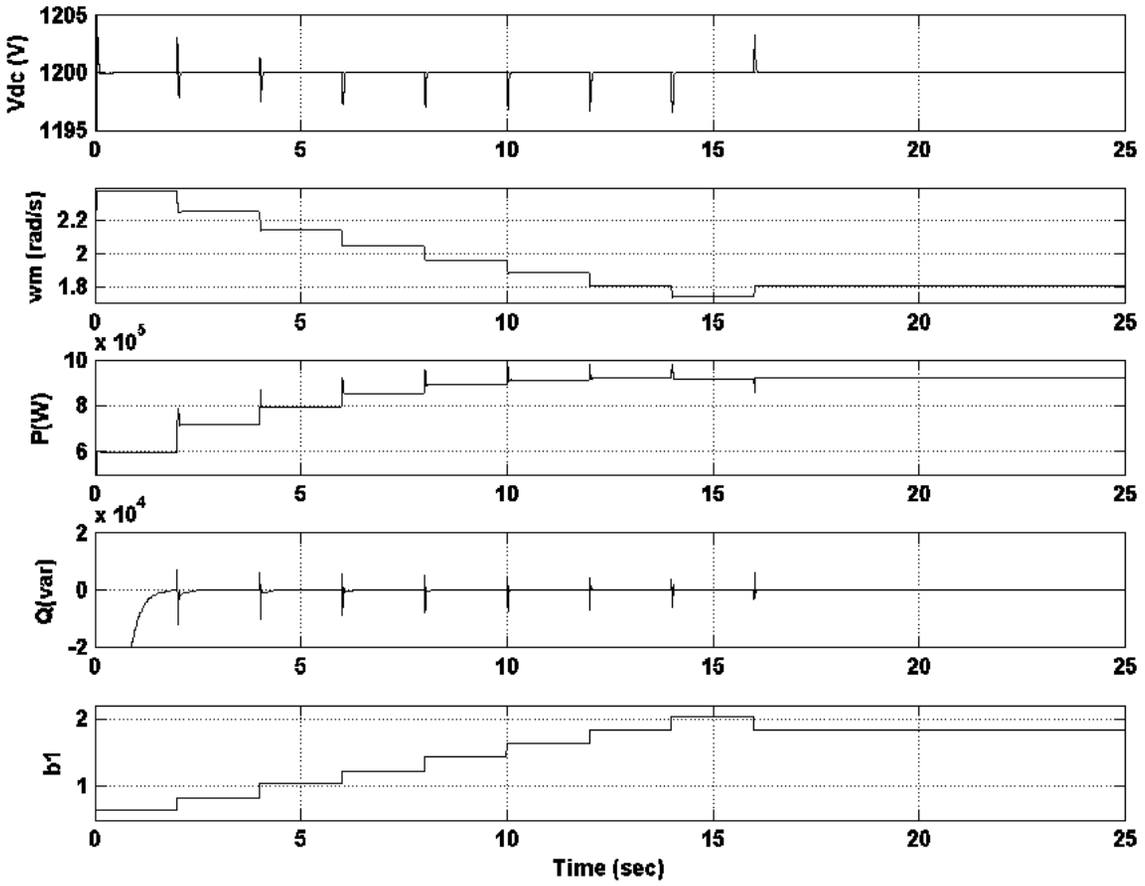

Figure 41. DFIG system operation applying the novel MPPT (simulation results)

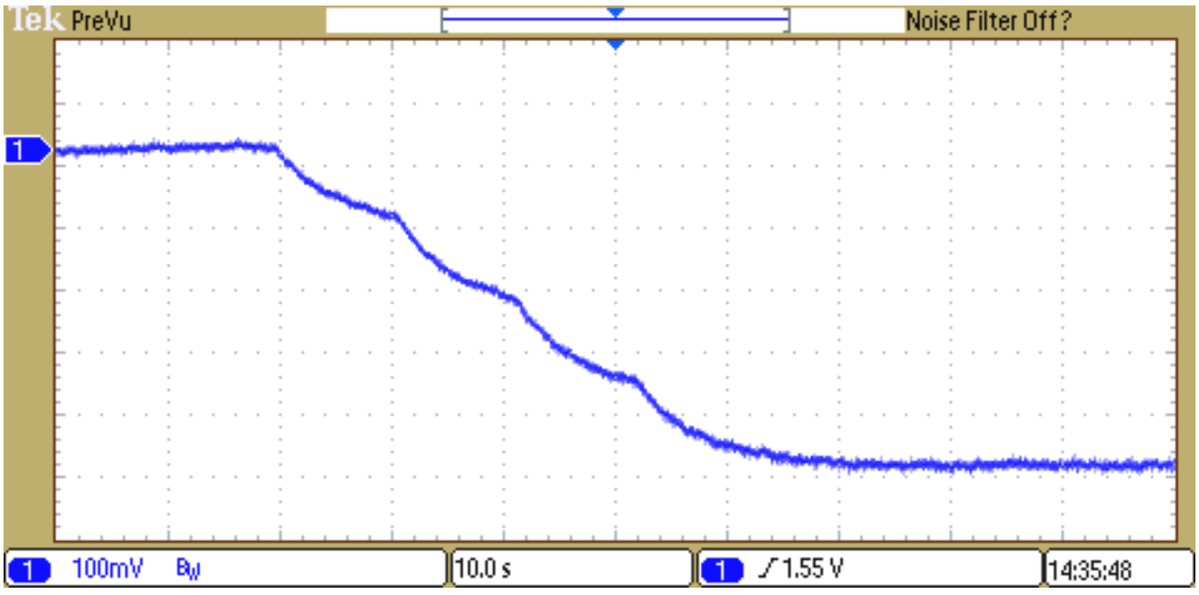

Figure 42. DFIG speed variation induced by the novel MPPT (experiment result)

4. Conclusion

Wind power systems have been widely studied and applied for years. By virtue of many advantages, induction generators are found to be suitable in this area. This chapter introduced and studied two popular types of induction generators – SCIG and DFIG. An overview of the generators, power electronics, and control strategies was presented first, followed by detailed modeling of entire wind system. Most importantly, the control algorithms were illustrated, ranging from FOC, SVM, PLL, to MPPT. Especially, different MPPT strategies were investigated and compared.

Acknowledgements

The contents of this chapter are the result of work at the Power Electronics Research Lab at the University of Akron, where my research was funded by Dr. Yilmaz Sozer; and work at the Renewable Energy Lab at Saginaw Valley State University, where my research was funded by the Faculty Research Grant.

I highly appreciate Dr. Yilmaz Sozer and Dr. Malik Elbuluk at the University of Akron for supervising my research work as well as guiding my progress in a peaceful and productive direction. I highly appreciate the support from Saginaw Valley State University that granted my start-up lab platform for long-term research commitment.

I am also very grateful to my wife, parents, and mother-in-law for their support. They established the foundation on which rests every success of my career.

Author details

Yu Zou*

Address all correspondence to: yzou123@svsu.edu

Saginaw Valley State University, Michigan, USA

References

[1] Stiebler M. *Wind Energy Systems for Electric Power Generation*. Rijeka: Springer; 2008, 14-26, 30-43.

[2] Ahlström A. *Simulating Dynamical Behaviour of Wind Power Structures*. Licentiate Thesis. Royal Institute of Technology; 2002, 7-20.

[3] Heier S. *Grid Integration of Wind Energy Conversion Systems*. Rijeka: John Wiley & Sons; 2006, 31-368.

[4] Walker J. Jenkins N. *Wind Energy Technology*. Rijeka: John Wiley & Sons; 1997.

[5] Boldea I. *The Electric Generators Handbook – Variable Speed Generators*. Rijeka: Taylor & Francis; 2006, I18- I28.

[6] Rüncos F., Carlson R., Sadowski N., Kuo-Peng P. Performance analysis of a doubly fed twin stator cage induction generator. In: Wiak S., Dems M., Komeza K. (eds.), *Recent Developments of Electrical Drives*. Rijeka: Springer; 2006, 361-373.

[7] Dubois M.R. *Optimized Permanent Magnet Generator Topologies for Direct-Drive Wind Turbines*. PhD Dissertation. Delft University Technology; 2004, 9-27.

[8] Rodrigo. Dissertation on Renewable Energy Sources. http://writepass.com/journal/2012/12/working-on-res-renewable-energy-sources/ (December 2012)

[9] Grauers A. *Design of Direct-Driven permanent-magnet generators for wind turbines. PhD Dissertation*. Chalmers University of Technology; 1996, 11-19, 37-55.

[10] Torrey D.A. Switched reluctance generators and their control. *IEEE Transact Indust Electron* 2002; 49(1) 3-14.

[11] Li H., Chen Z. Overview of different wind generator systems and their comparisons. *IET Renew Power Gen* 2008; 2(2) 123-138.

[12] Dubois M.R., Polinder H., Ferreira J.A. Comparison of generator topologies for direct-drive wind turbines. Proceedings of Nordic Countries Power and Industrial Electronics, NORPIE 2000 June 2000, Aalborg, Denmark, 22-26.

[13] Patil N.S., Bhosle Y.N. *A Review on Wind Turbine Generator Topologies.* International Conference on Power, Energy and Control, ICPEC 2013, 6-8 February 2013, Sri Rangalatchum Dindigul, 625-629.

[14] Lampola P. *Directly Driven, Low-Speed Permanent-Magnet Generators for Wind Power Applications*. PhD Dissertation. Helsinki University of Technology; 2000, 11-19.

[15] Siegfriedsen S., Bohmeke G. Multibrid technology – a significant step to multi-megawatt wind turbines. *Wind Energy* 1998; 1(2) 89-100.

[16] Polinder H., Van Der Pijl F.F.A., De Vilder G.J., Tavner P.J. Comparison of direct-drive and geared generator concepts for wind turbines. *IEEE Transact Energy Conver* 2006; 21(3) 725-733.

[17] Hansen L.H., Helle L., Blaabjerg F., Ritchie E., Munk-Nielsen S., Bindner H., Sørensen P., Bak-Jensen B. Conceptual survey of generators and power electronics for wind turbines. Riso National Laboratory Technical Report; 2001, 21-36, 46-50.

[18] Li H., Chen Z. Design optimization and evaluation of different wind generator systems. International Conference on Electrical Machines and Systems, ICEMS 2008, 17-20 October 2008, Wuhan, China, 2396-2401.

[19] Kanellos F.D., Papathanassiou S.A., Hatziargyriou N.D. Dynamic analysis of a variable speed wind turbine equipped with a voltage source AC/DC/A converter interface and a reactive current control loop. 10th Mediterranean Electrotechnical Conference, MELECON 2000, 29-31 May 2000, vol.3, 986-989.

[20] Chen Z., Guerrero J.M., Blaabjerg F. A review of the state of the art of power electronics for wind turbines. *IEEE Transact Power Electron* 2009; 24(8) 1859-1875.

[21] Baroudi J.A., Dinavahi V., Knight A.M. A review of power converter topologies for wind generators. IEEE International Conference on Electric Machines and Drives 2005, 15-15 May 2005, San Antonio, TX, USA, 458-465.

[22] Chen Z., Spooner E. Current source thyristor inverter and its active compensation system. *IEE Proc Gen, Trans Distrib* 2003; 150(4) 447-454.

[23] Zou Y., Elbuluk M., Sozer Y. A complete modeling and simulation of induction generator wind power systems. IEEE Industry Applications Society Annual Meeting, IAS 2010, 3-7 October 2010, Huston, TX, USA, 1-8.

[24] Tan K., Islam S. Optimum control strategies in energy conversion of PMSG wind turbine system without mechanical sensors. *IEEE Transact Energy Conver* 2004; 19(2) 392-399.

[25] Sun L., Mi Z., Yu Y., Wu T. Active power and reactive power regulation capacity study of DFIG wind turbine. International Conference on Sustainable Power Generation and Supply 2009, SUPERGEN 2009, 6-7 April 2009. Nanjing, China, 1-6.

[26] Schiemenz I., Stiebler M. Control of permanent magnet synchronous generator used in a variable speed wind energy system. IEEE International Electric Machines and Drives Conference, IEMDC 2001, 17-20 June 2001. Cambridge, MA, USA, 872-877.

[27] Hansen A.D., Michalke G. Multi-pole permanent magnet synchronous generator wind turbines' grid support capability in uninterrupted operation during grid faults. *IET Renew Power Gen* 2009; 3(3) 333-348.

[28] Ohyama K., Arinaga S., Yamashita Y. Modelling and simulation of variable speed wind generator system using boost converter of permanent magnet synchronous generator. European Conference on Power Electronics and Applications 2007, 2-5 September 2007, Aalborg, Denmark, 1-9.

[29] Keyuan H., Yikang H. Investigation of a matrix converter-excited brushless doubly-fed machine wind-power generation system. The 5th International Conference on Power Electronics and Drive Systems 2003, PEDS 2003, 17-20 November 2003, vol.1, 743-748.

[30] Zhang L., Watthanasarn C., Shepherd W. Application of a matrix converter for the power control of a variable-speed wind-turbine driving a doubly-fed induction generator. 23rd International Conference on Industrial Electronics, Control and Instrumentation 1997, IECON 1997, 9-14 November 1997, New Orleans, LA, USA, vol.2, 906-911.

[31] Singh M., Chandra A., Singh B. Sensorless power maximization of PMSG based isolated wind-battery hybrid system using adaptive neuro-fuzzy controller. IEEE Industry Applications Society Annual Meeting, IAS 2010, 3-7 October 2010, Huston, TX, USA, 1-6.

[32] Sozer Y. *Direct Adaptive Control Of Permanent Magnet Motors*. Ph.D Dissertation. Rensselaer Polytechnic Institute; 1999, 54-73.

[33] Zou Y. Modeling, *Control and Maximum Power Point Tracking (MPPT) of Doubly-Fed Induction Generator (DFIG) Wind Power System*. PhD Dissertation. University of Akron; 2012, 44-90.

[34] Bansal R. C. Automatic reactive-power control of isolated wind-diesel hybrid power systems. *IEEE Transact Indus Electron* 2006; 53(4) 1116-1126.

[35] Abo-Khalil A.G., Lee D.C. MPPT control of wind generation systems based on estimated wind speed using SVR. *IEEE Transact Indus Electron* 2008; 55(3) 1489-1490.

[36] Guo P. Research of a new MPPT strategy based on gray wind speed prediction. 2nd International Symposium on Knowledge Acquisition and Modelling 2009, KAM 2009, 30 November-1 December 2009. Wuhan, China, 120-123.

[37] Liu D., Wu Z., Wang H., Wang T. MPPT control strategy for off-grid wind power system. IEEE 2nd International Symposium on Power Electronics for Distributed Generation Systems 2010, PEDG 2010, 16-18 June 2010, Hefei, China, 759-764.

[38] Pan C., Juan Y. A novel sensorless MPPT controller for a high-efficiency microscale wind power generation system. *IEEE Transact Energy Conver* 2010; 25(1) 207-216.

[39] Jia Y., Yang Z., Cao B. A new maximum power point tracking control scheme for wind generation. International Conference on Power System Technology 2002, 13-17 October 2002. 144-148.

[40] Neammanee B., Krajangpan K., Sirisumrannukul S. Maximum peak power tracking-based control algorithms with stall regulation for optimal wind energy capture. Power Conversion Conference 2007, PCC 2007, 2-5 April 2007, Nagoya, 1424-1430.

[41] Koutroulis E., Kalaitzakis K. Design of a maximum power tracking system for wind-energy-conversion applications. *IEEE Transact Indus Electron* 2006; 53(2) 486-494.

[42] Wang P., Liu H., Guo C., Tao C. MPPT control algorithms for wind power generation based on voltage disturbance. 7th World Congress on Intelligent Control and Automation 2008, WCICA 2008, 25-27 June 2008, Chongqing, China, 7398-7402.

[43] Barote L., Marinescu C. Storage analysis for stand-alone wind energy applications. 12th International Conference on Optimization of Electrical and Electronic Equipment 2010, OPTIM 2010, 20-22 May 2010, Basov, 1180-1185.

[44] Fernandez L.M., Garcia C.A., Jurado F., Saebz H,R. Control system of doubly fed induction generators based wind turbines with production limits. IEEE International Conference on Electric Machines and Drives 2005, 15-15 May 2005, San Antonio, TX, USA, 1936-1941.

[45] Yuan X., Wang F., Boroyevich D., Li Y. DC-link voltage control of a full power converter for wind generator operating in weak-grid systems. *IEEE Transact Power Electron* 2009; 24(9) 2178-2192.

[46] Yang L., Yang G.Y., Xu Z., Dong Z.Y. Optimal controller design of a doubly-fed induction generator wind turbine system for small signal stability enhancement. *IET Gen, Trans Distrib* 2010; 4(5) 579-597.

[47] Zou Y., Elbuluk M., Sozer Y. *A Novel Maximum Power Points Tracking (MPPT) Operation of Doubly-Fed Induction Generator (DFIG) Wind Power System*. IEEE Industry Applications Society Annual Meeting, IAS 2012, 7-11 October 2012, Las Vegas, NV, USA, 1-6.

IntechOpen